Applied Chemical Engineering (2026) Volume 9 Issue 4 ISSN: 2578-2010 (O)
doi: 10.59429/ace.v9i4.6114

RESEARCH ARTICLE

Unsymmetrical A_3B-Type Phthalocyanines (Metal-Free and Metalated) and Their Polymeric Analogues: Synthesis, Structural Characterization, and Biological Activity Evaluation

Mays Saeed Obied, Mohanad Mousa Kareem*, Ahmed F. Halbus

Department of Chemistry, College of Science, University of Babylon, Babylon 51002, Iraq

***Corresponding author:** Mohanad Mousa Kareem, sci.mohanad.mousa@uobabylon.edu.iq

ABSTRACT

The prepared phthalocyanine derivatives and their polymeric analogues were investigated using FT-IR, ^{1}H NMR, and UV–visible spectroscopy. GPC measurements were available for the metal-free and nickel-containing polymeric products and indicated narrow apparent molar-mass distributions. The antibacterial activity of polymeric compounds 8–14 was evaluated against Staphylococcus aureus and Escherichia coli using the agar diffusion method. Reported inhibition zones ranged from 10 to 17 mm for S. aureus and from 10 to 18 mm for E. coli. These observations support further investigation of the materials, while additional analytical evidence is needed to establish the proposed A_3B composition and purity.

Keywords: Unsymmetrical phthalocyanines; Metallophthalocyanines; Cyclotetramerization; Maleimide; Antibacterial activity; Staphylococcus aureus; Escherichia coli; Spectroscopic characterization.

ARTICLE INFO

Received: 06 July 2026
Accepted: 20 October 2026
Available online: 04 November 2026

COPYRIGHT

Copyright © 2026 by author(s).
Applied Chemical Engineering is published by Arts and Science Press Pte. Ltd. This work is licensed under the Creative Commons Attribution-NonCommercial 4.0 International License (CC BY 4.0).
https://creativecommons.org/licenses/by/4.0/

1. Introduction

Phthalocyanines are conjugated macrocycles that have been investigated in photocatalysis [1], gas-sensing composites [2], and photodynamic therapy [3]. Antimicrobial photodynamic studies have evaluated zinc phthalocyanine derivatives against bacterial pathogens [4,5]. Unsymmetrical A_3B-type phthalocyanines provide distinct peripheral functions within one macrocycle; related studies include thiazolidin-4-one-substituted zinc derivatives [6], amphiphilic A_3B derivatives [7], and a zinc phthalocyanine initiator for poly(ε-caprolactone) synthesis [8]. Other functionalized zinc phthalocyanines bearing dodecenyl succinic anhydride benzoic groups have also been reported [9].

Antimicrobial resistance motivates research into alternative antibacterial approaches. Literature studies discuss methicillin-resistant *Staphylococcus aureus* [10] and multidrug-resistant *Pseudomonas aeruginosa* [11]; the latter is cited here as resistance background and was not tested in the present work. Phthalocyanine-mediated photodynamic inactivation is discussed in the literature [12], and photochemical properties have also been investigated for phosphorus(V) phthalocyanines [13]. These light-dependent findings do not establish a photodynamic mechanism for the present agar diffusion results, for which a controlled irradiation protocol was not reported.

The two bacterial species tested here represent different cell-envelope structures. *Staphylococcus aureus* is Gram-positive and has

a multilayered peptidoglycan cell wall, whose architecture has been investigated experimentally [14]. Resistance status was not established for the *S. aureus* used in the present study.

Escherichia coli was included as the Gram-negative test organism. The present inhibition-zone measurements allow comparison with *S. aureus* but do not establish bacterial resistance status, a specific cellular target, or an antibacterial mechanism.

Related antibacterial research has investigated alkyl-chain-modified phthalocyanines doped with Ag^{+} and Pd^{2+} ions [15], Schiff-base morpholino phthalocyanines under photodynamic conditions [16], and gallic-acid-anchored phthalocyanine-doped silica nanoparticles against planktonic cells and biofilms [17]. These systems provide context for the present screening study, but their different formulations and assay conditions prevent direct attribution of their mechanisms to compounds 8–14. Polymer-supported phthalocyanines have also been studied: an A_3B-type zinc phthalocyanine was used as an initiator for ring-opening polymerization of ε-caprolactone [8].

The present work examines the synthesis and characterization of proposed unsymmetrical phthalocyanine derivatives and their polymeric analogues, together with agar diffusion screening of the polymeric products against *S. aureus* and *E. coli*. Previous studies of amphiphilic carboxyl phthalocyanine oligomers [18], symmetrical and unsymmetrical zinc phthalocyanines [19], and aldehyde-substituted metal-free and nickel phthalocyanines [20] provide related examples of phthalocyanine synthesis and characterization.

2. Experimental

2.1. Materials and techniques

Analytical-grade solvents and reagents were obtained from Fluka, Sigma-Aldrich, CDH, and Riedel-de Haën. ATR-FT-IR spectra were recorded over 400–4000 cm^{-1} using a Shimadzu FT-IR spectrometer. UV absorption measurements were performed using a PG CECIL CE7200 double-beam spectrophotometer. ^1H NMR spectra were recorded using a Varian INOVA 500 MHz spectrometer in DMSO-d_6, with TMS as the reference standard. Chemical shifts are reported in parts per million (ppm).

2.2. Synthesis methods

2.2.1. Preparation of the maleimide-functionalized phthalonitrile precursor

Maleic anhydride (3.268 g) and 4-aminophthalonitrile (4.771 g) were mixed in DMF (10 mL), and phosphoric acid (H_3PO_4; 2–3 drops) was added. The mixture was heated under reflux with stirring for 2 h. The reaction mixture was then added to cold distilled water, and the resulting product was recrystallized from ethanol to obtain 4-(2,5-dioxo-2,5-dihydro-1H-pyrrol-1-yl)phthalonitrile.

2.2.2. Synthesis of metal-free and metalated phthalocyanines

4-Aminophthalonitrile (0.481 g), 4-(2,5-dioxo-2,5-dihydro-1H-pyrrol-1-yl)phthalonitrile (0.250 g), and ammonium molybdate (0.038 g) were ground together with urea (1.300 g). The molar ratio of 4-aminophthalonitrile to the maleimide-functionalized phthalonitrile precursor was 3:1. For the metalated derivatives, the corresponding metal(II) chloride was included: cobalt(II) chloride (0.338 g), zinc(II) chloride (0.334 g), copper(II) chloride (0.350 g), magnesium(II) chloride (0.247 g), nickel(II) chloride (0.337 g), or iron(II) chloride (0.329 g). The temperature was increased gradually to 200 °C, and the reaction mixture was maintained in the molten state at this temperature for 20 min. The products were recrystallized from DMF to afford compounds 1–7 (Scheme 1).

Individual characterization data for compounds 1–7

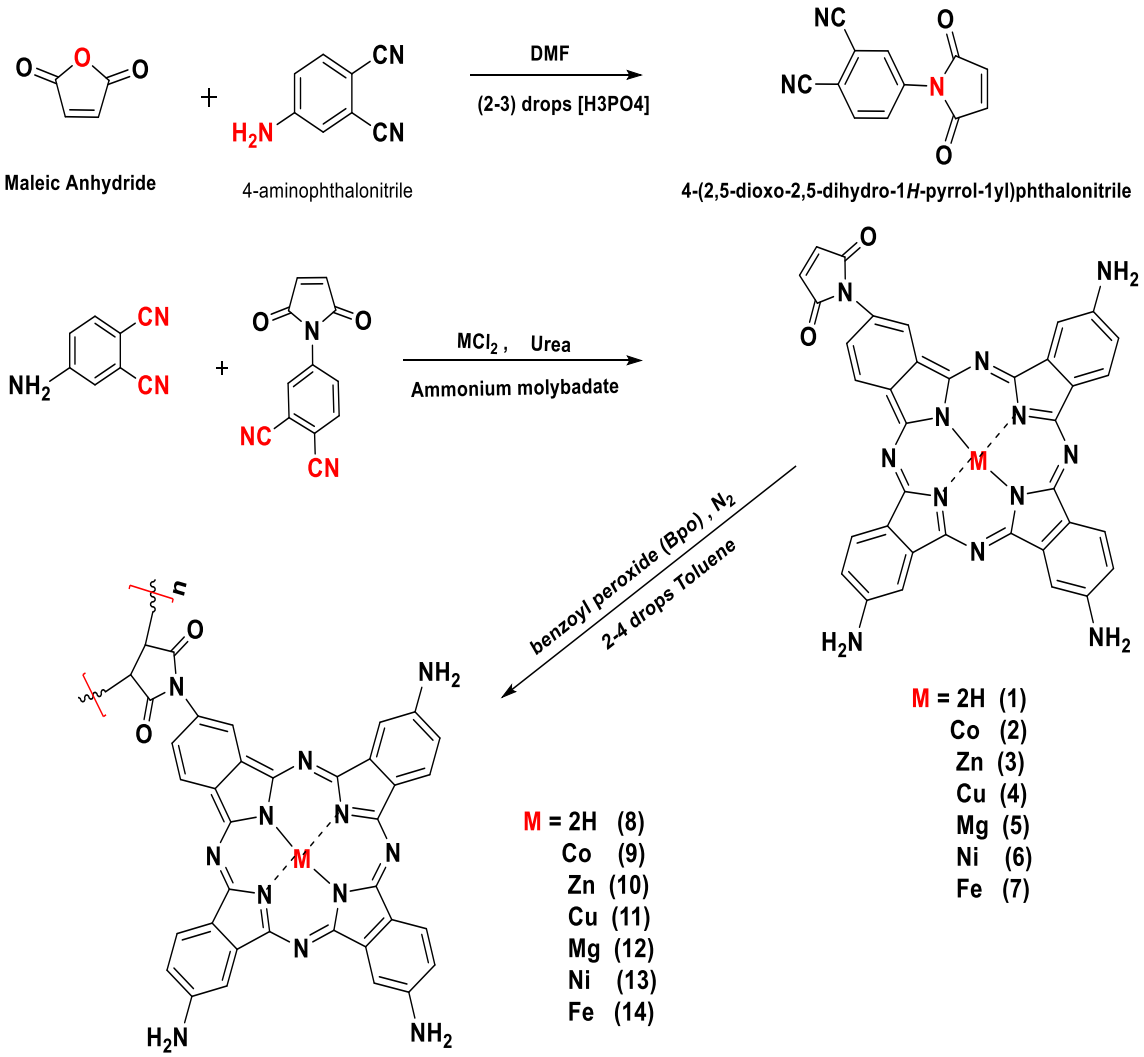
Compounds 1–7 were purified by recrystallization from DMF, as described above. Individual physical and spectroscopic data are summarized below. Compound 1 (Pc–H_2). Greenish-yellow product; yield 73%; m.p. 280.3 °C. FT-IR (ATR, cm^{-1}): 3350.35, 1616.35–1454.33, 1159.22. UV–Vis: λmax = 694.5 nm. The FT-IR and ^1H NMR spectra are provided in Figures S3 and S17, respectively. Compound 2 (Pc–Co). Green product; yield 76%; m.p. 291.1 °C. FT-IR (ATR, cm^{-1}): 3360.00, 1622.13–1456.26, 1159.22. UV–Vis: λmax = 676.0 nm. The FT-IR and ^1H NMR spectra are provided in Figures S4 and S18, respectively.

Compound 3 (Pc–Zn). Olive product; yield 78%; m.p. 291.3 °C. FT-IR (ATR, cm^{-1}): 3452.58, 1620.21–1458.18, 1155.36. UV–Vis: λmax = 691.5 nm. The FT-IR and ^1H NMR spectra are provided in Figures S5 and S19, respectively. Compound 4 (Pc–Cu). Dark-olive product; yield 75%; m.p. 287.8 °C. FT-IR (ATR, cm^{-1}): 3344.57, 1622.13–1456.26, 1155.36. UV–Vis: λmax = 679.0 nm. The FT-IR and ^1H NMR spectra are provided in Figures S6 and S20, respectively.

Compound 5 (Pc–Mg). Dark-green product; yield 80%; m.p. 289.1 °C. FT-IR (ATR, cm^{-1}): 3354.21, 1622.00–1458.18, 1159.22. UV–Vis: λmax = 677.0 nm. The FT-IR and ^1H NMR spectra are provided in Figures S7 and S21, respectively. Compound 6 (Pc–Ni). Very dark-green product; yield 76%; m.p. 292.5 °C. FT-IR (ATR, cm^{-1}): 3344.57, 1623.67–1456.26, 1157.29. UV–Vis: λmax = 695.0 nm. The FT-IR and ^1H NMR spectra are provided in Figures S8 and S22, respectively. Compound 7 (Pc–Fe). Very light-green product; yield 84%; m.p. 288.2 °C. FT-IR (ATR, cm^{-1}): 3350.35, 1622.13–1456.26, 1157.29. UV–Vis: λmax = 694.0 nm. The FT-IR and ^1H NMR spectra are provided in Figures S9 and S23, respectively.

2.2.3. Preparation of polymeric phthalocyanine analogues

Monomers 1–7 were polymerized separately. The masses of Pc–H_2 (1), Pc–Co (2), Pc–Zn (3), Pc–Cu (4), Pc–Mg (5), Pc–Ni (6), and Pc–Fe (7) were 1.096, 1.192, 1.204, 1.200, 1.136, 1.192, and 1.1880 g, respectively. Each monomer was mixed in a separate test tube with the corresponding mass of benzoyl peroxide (BPO): 0.382, 0.400, 0.420, 0.396, 0.400, 0.410, and 0.206 g, respectively, and 2–4 drops of toluene. Each tube was flushed with nitrogen for 10 min, loosely closed, and maintained in a water bath at 90 °C for 3 h. The solvent was then evaporated, and the resulting product was washed with diethyl ether and dried in an oven at 50 °C. Monomers 1–7 afforded the corresponding polymeric products 8–14, respectively (Scheme 1). In radical chain polymerization, initiator-derived active centres enable successive addition of monomer units [21]; the detailed chain structure of the present products nevertheless requires independent analytical confirmation.



Scheme 1. Synthesis of monomeric compounds 1–7 and their polymeric analogues 8–14.

Individual characterization data for compounds 8–14

Compounds 8–14 were washed with diethyl ether and dried at 50 °C, as described above. Individual physical and spectroscopic data are summarized below.Compound 8 (Polymer–H_2). Brown, sticky product obtained from monomer 1; yield 71%. FT-IR (ATR, cm^{-1}): 3435.22, 1674.21–1450.47, 1126.43. UV–Vis: λmax = 697.0 nm. GPC: Mn ≈ 3659 g mol^{-1}; Mw ≈ 3854 g mol^{-1}; Đ ≈ 1.05. The FT-IR spectrum and GPC chromatogram are provided in Figures S10 and S24, respectively. The ^{1}H NMR spectrum is provided in Figure S26. Compound 9 (Polymer–Co). Dark-green, sticky product obtained from monomer 2; yield 69%. FT-IR (ATR, cm^{-1}): 3451.32, 1622.13–1450.47, 1124.13. UV–Vis: λmax = 696.5 nm. The FT-IR spectrum is provided in Figure S11. The ^{1}H NMR spectrum is provided in Figure S27.

Compound 10 (Polymer–Zn). Dark-olive, sticky product obtained from monomer 3; yield 68%. FT-IR (ATR, cm^{-1}): 3462.22, 1653.00–1438.90, 1095.57. UV–Vis: λmax = 697.5 nm. The FT-IR spectrum is provided in Figure S12. The ^{1}H NMR spectrum is provided in Figure S28.

Compound 11 (Polymer–Cu). Dark-olive, sticky product obtained from monomer 4; yield 72%. FT-IR (ATR, cm^{-1}): 3421.72, 1670.35–1406.11, 1022.27. UV–Vis: λmax = 700.0 nm. The FT-IR spectrum is provided in Figure S13. The ^{1}H NMR spectrum is provided in Figure S29.

Compound 12 (Polymer–Mg). Dark-green, sticky product obtained from monomer 5; yield 71%. FT-IR (ATR, cm^{-1}): 3461.13, 1622.13–1467.83, 1161.15. UV–Vis: λmax = 698.0 nm. The FT-IR spectrum is provided in Figure S14. The ^{1}H NMR spectrum is provided in Figure S30.

Compound 13 (Polymer–Ni). Dark-green, sticky product obtained from monomer 6; yield 71%. FT-IR (ATR, cm^{-1}): 3433.29, 1622.13–1450.47, 1074.35. UV–Vis: λmax = 695.5 nm. GPC: Mn ≈ 3530 g mol^{-1}; Mw ≈ 3732 g mol^{-1}; Đ ≈ 1.06. The FT-IR spectrum and GPC chromatogram are provided in Figures S15 and S25, respectively. The ^1H NMR spectrum is provided in Figure S31.

Compound 14 (Polymer–Fe). Dark-olive, sticky product obtained from monomer 7; yield 70%. FT-IR (ATR, cm^{-1}): 3441.37, 1622.13–1450.47, 1124.50. UV–Vis: λmax = 695.0 nm. The FT-IR spectrum is provided in Figure S16. The ^1H NMR spectrum is provided in Figure S32.

Table 1. Physical properties and yields of compounds 1–14.

Compound	Melting point (°C)	Color	Yield (%)	Solubility				
				H_2O	C_2H_6O	DMSO	CH_3OH	$(CH_3)_2CO$
Pc–H_2 (1)	280.3	Greenish yellow	73%	-	P	+	P	P
Pc–Co (2)	291.1	green	76%	-	P	+	P	P
Pc–Zn (3)	291.3	Olive	78%	-	P	+	P	P
Pc–Cu (4)	287.8	dark olive	75%	-	P	+	P	P
Pc–Mg (5)	289.1	Dark green	80%	-	P	+	P	P
Pc–Ni (6)	292.5	very dark green	76%	-	P	+	P	P
Pc–Fe (7)	288.2	Very light green	84%	-	P	+	P	P
Polymer–H_2 (8)	Sticky	brown	71%	-	P	+	P	P
Polymer–Co (9)	Sticky	dark green	69%	-	P	+	P	P
Polymer–Zn (10)	Sticky	dark olive	68%	-	P	+	P	P
Polymer–Cu (11)	Sticky	dark olive	72%	-	P	+	P	P
Polymer–Mg (12)	Sticky	dark green	71%	-	P	+	P	P
Polymer–Ni (13)	Sticky	dark green	71%	-	P	+	P	P
Polymer–Fe (14)	Sticky	dark olive	70%	-	P	+	P	P

P = partially soluble; + = soluble; − = insoluble.

2.3. Antibacterial activity

The antibacterial activity of polymeric compounds 8–14 was investigated against *Staphylococcus aureus* and *Escherichia coli* using the agar diffusion method. Each sample (0.0004 g) was dissolved in 2 mL of DMSO, corresponding to a nominal concentration of 0.2 mg mL^{-1}. The solutions were added to wells in inoculated agar plates. After incubation for 24 h at 37 °C, inhibition-zone diameters were measured. The recorded results are provided in Table 3 of the main text and Table S1 of the Supporting Information; plate images are shown in Images S1 and S2 of the Supporting Information. DMSO alone was used as the negative control and showed no detectable antibacterial activity against either *S. aureus* or *E. coli*.

3. Results and discussion

3.1. FT-IR spectroscopy

The FT-IR spectra of compounds 1–14 are provided in Figures S3–S16 of the Supporting Information, and selected bands are summarized in Table 2. Monomers 1–7 exhibit high-wavenumber bands at 3344.57–3452.58 cm^{-1} and bands in the 1454.33–1623.67 cm^{-1} region. The polymeric products show corresponding high-wavenumber bands at 3421.72–3462.22 cm^{-1} and bands in the 1406.11–1674.21 cm^{-1} region. Bands assigned to C–N vibrations occur at 1155.36–1159.22 cm^{-1} for the monomers and 1022.27–1161.15 cm^{-1} for

the polymeric products. The values grouped under C=O, C=C, and C=N in Table 2 are reported spectral ranges; individual vibrations cannot be assigned from these ranges alone. In particular, the imide carbonyl assignment requires examination of the complete spectra. The cobalt spectrum (Figure S4) shows labelled bands at 1622.13 and 1456.26 cm^{-1}. A comparison with an independently characterized precursor is required to establish disappearance of the nitrile band during cyclotetramerization. The available product spectra alone do not establish selective formation or purity of the proposed A_3B product, and low-wavenumber bands should not be treated as definitive evidence of metal coordination without supporting assignments. FT-IR is also used to examine functional groups in other materials, including green-synthesized nanoparticles [22]; its diagnostic interpretation must remain specific to the sample and supported by complementary evidence.

Table 2. Selected FT-IR bands of compounds 1–14.

Compound	High-wavenumber band (cm^{-1})	C=O, C=C, C=N (cm^{-1})	C–N (cm^{-1})
Pc–H_2 (1)	3350.35	1616.35-1454.33	1159.22
Pc–Co (2)	3360.00	1622.13–1456.26	1159.22
Pc–Zn (3)	3452.58	1620.21-1458.18	1155.36
Pc–Cu (4)	3344.57	1622.13-1456.26	1155.36
Pc–Mg (5)	3354.21	1622.00-1458.18	1159.22
Pc–Ni (6)	3344.57	1623.67-1456.26	1157.29
Pc–Fe (7)	3350.35	1622.13-1456.26	1157.29
Polymer–H_2 (8)	3435.22	1674.21-1450.47	1126.43
Polymer–Co (9)	3451.32	1622.13-1450.47	1124.13
Polymer–Zn (10)	3462.22	1653.00-1438.90	1095.57
Polymer–Cu (11)	3421.72	1670.35-1406.11	1022.27
Polymer–Mg (12)	3461.13	1622.13-1467.83	1161.15
Polymer–Ni (13)	3433.29	1622.13-1450.47	1074.35
Polymer–Fe (14)	3441.37	1622.13-1450.47	1124.50

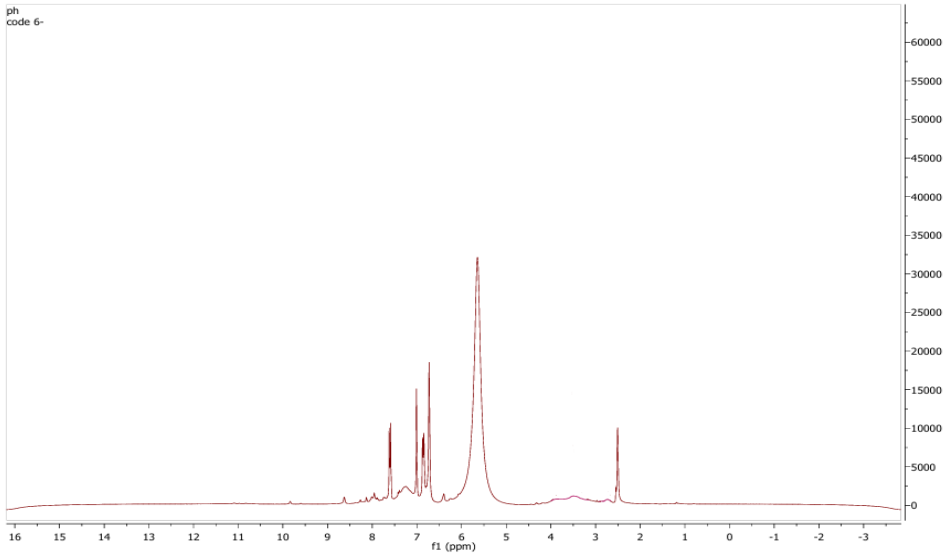
3.2. ^{1}H NMR spectroscopy

The ^{1}H NMR spectra of monomeric phthalocyanines 1–7 are presented in Figures S17–S23 of the Supporting Information. The measurements were recorded in DMSO-d_6, with the residual solvent resonance at approximately δ 2.50 ppm. The monomer spectra are discussed separately from those of the polymeric analogues. Reported resonances in the aromatic region occur at δ 7.45–9.06 ppm. Because the proposed maleimide proton resonances overlap this region, their assignment cannot be based on chemical shift alone. Compound-specific assignments require resolved resonances and supporting integration. The spectra labelled for the metal-containing compounds should therefore be interpreted individually, rather than assigning the same chemical-shift ranges to every compound. Spectral interpretation requires attention to chemical-shift assignments and other diagnostic information [23]. Self-association has been studied by NMR in asymmetrically substituted phthalocyanines [24], and aggregation behaviour has also been examined in related phthalocyanine and naphthalocyanine derivatives [25]. These literature observations do not identify the cause of any particular feature in the present spectra.

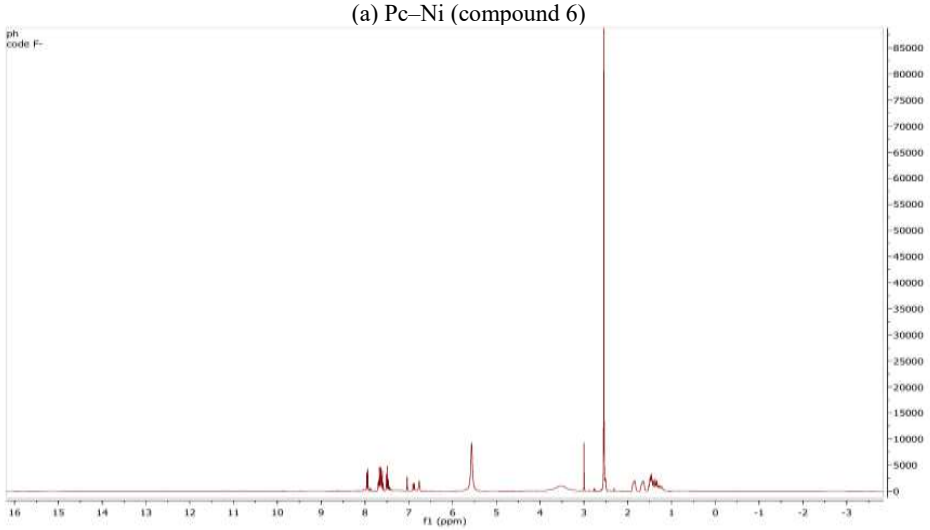
The magnetic properties of metal-containing phthalocyanines require compound-specific consideration. Diamagnetic behaviour has been measured for a substituted Ni(II) phthalocyanine [26], whereas planar Co(II) and Cu(II) phthalocyanines have been reported as paramagnetic [27]. Ni-containing derivatives should therefore not be classified as paramagnetic solely by grouping them with Co-containing derivatives. Nevertheless, paramagnetism does not invariably prevent observation of an NMR spectrum: resolved spectra have been reported for suitably substituted Co(II) phthalocyanines when aggregation and stacking were suppressed [28].

Thus, metal identity alone does not establish the origin of broadening or the validity of an assignment. The present spectra are not accompanied by magnetic-susceptibility or relaxation measurements. The oxidation and spin states of the Fe-containing products also require independent confirmation. No compound-specific spin-state determination is claimed here, and the Co-, Cu-, and Fe-containing spectra are not treated as fully assigned structural proof.

The individual spectra of polymeric analogues 8–14 are presented in Figures S26–S32 of the Supporting Information. Figure 1 compares the supplied spectra of Pc–Ni (6) and Polymer–Ni (13). Compared with the monomers, changes in the olefinic region and the presence of resonances in the aliphatic region may support consumption of the maleimide double bond during polymerization. However, the available images do not establish complete disappearance of an individually assigned maleimide resonance for every monomer–polymer pair. Signals in the δ 1.5–2.0 ppm region should not be attributed exclusively to the polymer backbone without excluding residual reagents and solvents. The comparison in Figure 1 displays the spectral differences, but does not provide an independently assigned, integrated maleimide resonance from which conversion can be quantified. The present spectra provide qualitative information, but complete assignments and a definitive assessment of conversion require the original spectra and integration data.



(a) Pc–Ni (compound 6)



(b) Polymer–Ni (compound 13)

Figure 1. Comparison of the supplied ^{1}H NMR spectra of (a) Pc–Ni (6) and (b) Polymer–Ni (13). The displayed chemical-shift axes are retained from the original images. The spectra are shown on their original independent intensity scales and are not normalized. Individual polymer spectra are provided in Figures S26–S32.

3.3. U.V-visible absorption the prepared phthalocyanines

The Q- band covering 600–750 nm is known as the Q band of phthalocyanine and is formed due to (π-π*) transitions (HOMO–LUMO transition) of the phthalocyanine moieties [18,29].

The electronic absorption spectra of the synthesized phthalocyanine compounds are presented in figure 2. All compounds exhibited a characteristic Q-band in the visible region, with absorption maxima ranging from 676.0 to 695.0 nm, corresponding to the π→π* electronic transitions within the highly conjugated phthalocyanine macrocycle. The metal-free phthalocyanine (H_2Pc) displayed an absorption maximum at 694.5 nm, while the metallophthalocyanine complexes exhibited absorption maxima at 676.0 nm for CoPc, 691.5 nm for ZnPc, 679.0 nm for CuPc, 677.0 nm for MgPc, 695.0 nm for NiPc, and 694.0 nm for FePc.

The slight variations in the absorption maxima among the synthesized compounds can be attributed to the influence of the coordinated metal ions on the electronic distribution within the phthalocyanine macrocycle. Despite these minor shifts, all complexes retained the characteristic π→π* transition, confirming the successful formation of the phthalocyanine framework and the preservation of its extended π-conjugated electronic system.

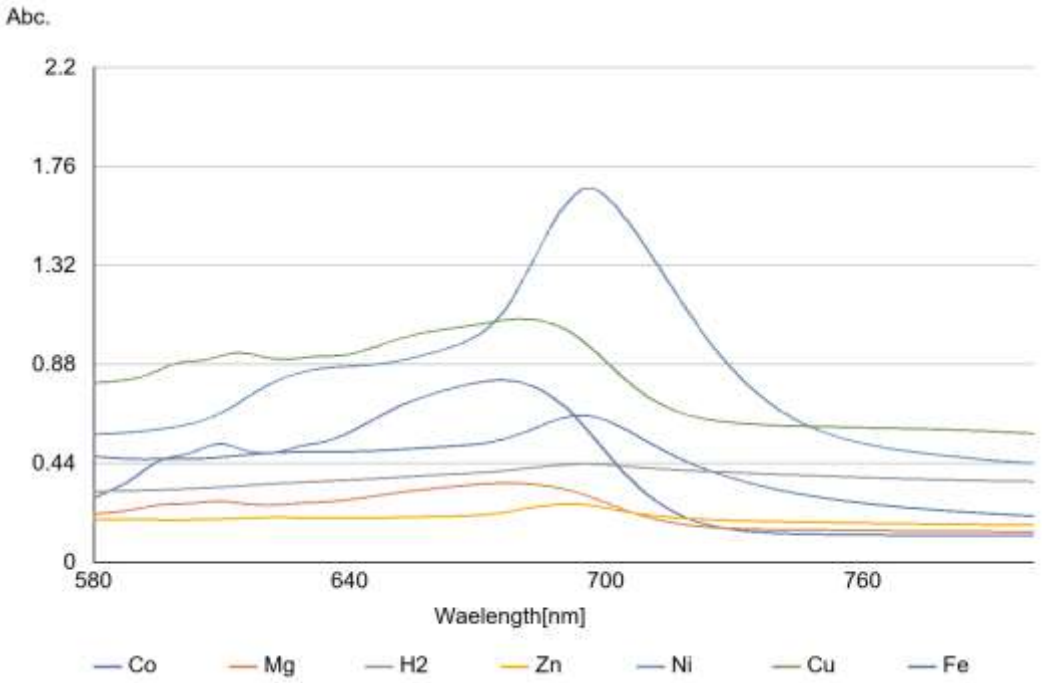


Figure 2. UV-Vis spectra of compounds 1-7

The electronic spectral data (figure 3) of the free polymer and its metal complexes show a single broad absorption band in the range of 695–700 nm, which is assigned to π → π* electronic transitions within the conjugated polymer backbone. The presence of absorption in the visible region confirms an extended conjugation system in the polymer structure, indicating a highly delocalized π-electron system with good electronic stability. A comparison between the free polymer and its metal complexes shows only minor shifts in the absorption maxima, indicating that metal coordination does not significantly disturb the conjugated framework but only slightly modifies the electronic environment through metal–ligand interactions.

The Cu complex shows a red shift to 700 nm, suggesting a slight stabilization of the excited state and stronger interaction between the metal ion and the conjugated system. The Ni and Fe complexes show slight blue shifts to 695.5 nm and 695 nm, indicating a small increase in transition energy. The Zn, Mg, and Co complexes exhibit absorption bands very close to the free polymer, reflecting minimal electronic disturbance.

Overall, the results indicate that metal coordination preserves the main π-conjugated system of the polymer while introducing only subtle electronic variations depending on the nature of the metal ion.

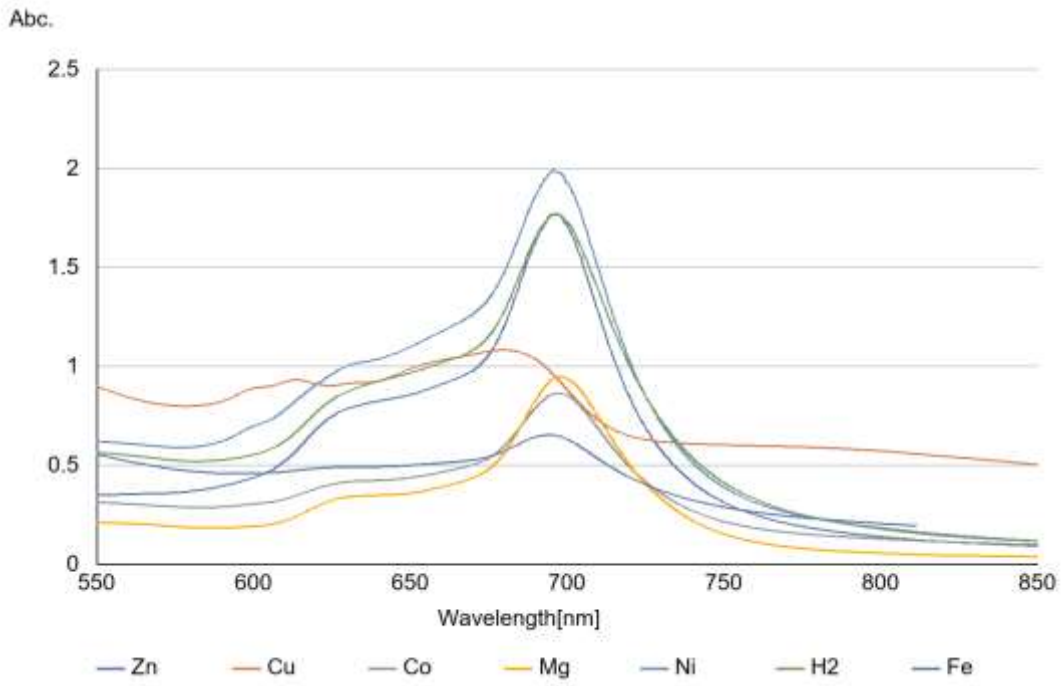


Figure 3. UV-Vis spectra of compounds 8-14

3.4. Gel permeation chromatography

3.4.1. GPC analysis of Polymer – H_2 (compound 8)

The GPC report for Polymer–H₂ (8) (Figure S24) shows a principal peak at a retention time of approximately 9.32 min. The reported number-average and weight-average molar masses are Mn ≈ 3659 g mol⁻¹ and Mw ≈ 3854 g mol⁻¹, respectively, giving Đ = Mw/Mn ≈ 1.0533 (approximately 1.05). This indicates a narrow apparent molar-mass distribution under the measurement conditions. A single chromatographic peak does not establish chemical purity or exclude co-eluting species.

The approximate number-average degree of polymerization (DPn) was estimated using the proposed repeat-unit molar mass (M_0 = 654.2 g mol⁻¹) [30]:

$$DP = \frac{M_w}{M_0} = \frac{3854}{654.2} \approx 5.89$$

Using the proposed repeat-unit molar mass of 654.2 g mol⁻¹, DPn ≈ Mn/M_0 = 3659/654.2 ≈ 5.59, corresponding to approximately six repeat units. This estimate depends on the proposed repeat-unit composition and the GPC calibration [30].

3.4.2. GPC analysis of Polymer – Ni (compound 13)

The GPC report for Polymer–Ni (13) (Figure S25) shows a principal peak at a retention time of approximately 9.33 min. The reported 100% integrated peak area refers to the peak included in the chromatographic integration and should not be interpreted as 100% chemical purity.

The reported dispersity of Polymer–Ni (13) is Đ ≈ 1.0573 (approximately 1.06), consistent with a narrow apparent molar-mass distribution under the measurement conditions.

GPC data were available for Polymer–H_2 (8) and Polymer–Ni (13) only. These measurements describe their apparent molar-mass distributions; they do not independently confirm the proposed molecular structures or the absence of all by-products. Complementary characterization has been used in related materials: fluorescent polyamides were examined using spectroscopic, morphological, and thermal methods [31], while symmetrical and unsymmetrical zinc phthalocyanines have been studied for their thermal properties [19]. Such results are examples from other systems and are not thermal measurements of the present products.

For Polymer–Ni (13), the reported values are Mn ≈ 3530 g mol^{-1} and Mw ≈ 3732 g mol^{-1}, with Đ = Mw/Mn ≈ 1.0573.

The approximate number-average degree of polymerization (DPn) was estimated using the proposed repeat-unit molar mass (M_0 = 711.32 g mol^{-1}) [30]:

$$DP = \frac{Mw}{M_0} = \frac{3732}{711.32} \approx 5.24$$

Using the proposed repeat-unit molar mass of 711.32 g mol^{-1}, DPn ≈ 3530/711.32 ≈ 4.96, corresponding to approximately five repeat units [30].

4. Antibacterial activity

4.1. Antibacterial activity of polymeric compounds 8 – 14

The antibacterial results for polymeric compounds 8–14 are summarized in Table 3, Table S1, and Figure 4. Reported inhibition-zone diameters were 10–17 mm for *S. aureus* and 10–18 mm for *E. coli*. The reference antibiotic ranges in Table S1 were 21–28 mm and 14–16 mm for ampicillin against *S. aureus* and *E. coli*, respectively, and 22–24 mm and 14–19 mm for amoxicillin. These ranges are reported as provided; their midpoints should not be treated as replicate-based means, and standard deviations cannot be calculated without the individual measurements.

Table 3. Reported antibacterial inhibition-zone diameters for polymeric compounds 8–14.

Polymeric compound	*Staphylococcus aureus (mm)*	*Escherichia coli (mm)*
Polymer–H_2 (8)	17	15
Polymer–Co (9)	15	15
Polymer–Zn (10)	10	10
Polymer–Cu (11)	15	18
Polymer–Mg (12)	10	12
Polymer–Ni (13)	12	13
Polymer–Fe (14)	15	15

Negative control: DMSO alone showed no detectable inhibition against either bacterial species. A numerical inhibition-zone diameter was not provided.

For *S. aureus*, the reported inhibition zones for compounds 8–14 were 17, 15, 10, 15, 10, 12, and 15 mm, respectively. For *E. coli*, the corresponding values were 15, 15, 10, 18, 12, 13, and 15 mm. Polymer–H_2 (8) had the largest reported zone against *S. aureus*, whereas Polymer–Cu (11) had the largest against *E. coli*. These findings describe the observed agar-diffusion response under the reported conditions; they do not establish a mechanism of action or statistical significance.

The reported inhibition zones vary with both the polymeric sample and the bacterial species. DMSO alone showed no detectable antibacterial activity against either tested species. Without replicate-level measurements,

the relative activities should be interpreted descriptively. Additional controlled measurements are needed before assigning the differences specifically to the coordinated metal ion. Replicate-level results, bacterial strain identifiers, well diameters, and the volume applied per well were not available in the supplied records. The results are therefore presented as preliminary screening observations; inhibition-zone diameters alone do not establish bactericidal activity or minimum inhibitory concentrations.

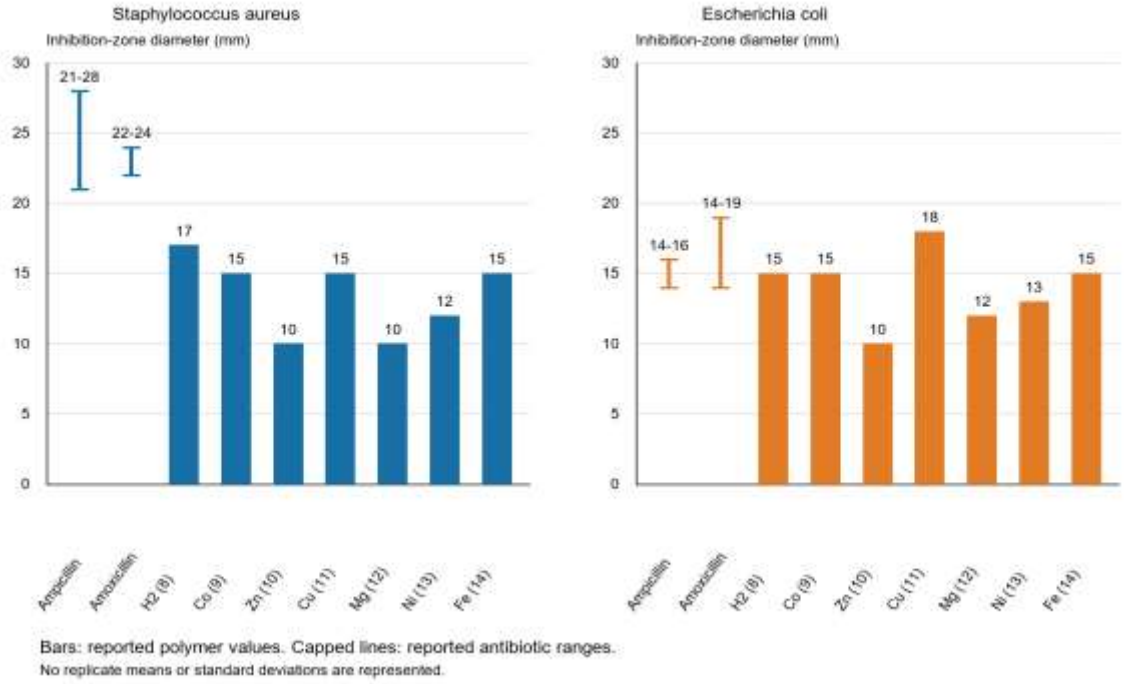


Figure 4. Reported antibacterial inhibition-zone diameters for polymeric compounds 8–14 against *Staphylococcus aureus* (left) and *Escherichia coli* (right). Bars represent the recorded polymer values, and capped lines show the antibiotic ranges reported in Table S1. The capped lines do not represent standard deviations. No replicate means or statistical error bars are shown.

5. Conclusions

Phthalocyanine derivatives and their polymeric analogues were prepared and investigated using FT-IR, ^{1}H NMR, and UV–visible spectroscopy. The available spectra provide supporting information, but do not independently establish selective formation and purity of the proposed unsymmetrical A_3B products. GPC measurements for Polymer–H_2 (8) and Polymer–Ni (13) indicated narrow apparent molar-mass distributions, with dispersities of approximately 1.05 and 1.06 and estimated degrees of polymerization of approximately six and five, respectively. The antibacterial assays reported for polymeric compounds 8–14 showed inhibition zones against *S. aureus* and *E. coli*. Polymer–H_2 (8) gave the largest reported zone against *S. aureus*, and Polymer–Cu (11) gave the largest against *E. coli*. Further structural characterization and controlled biological measurements are required to assess molecular identity, purity, reproducibility, and mechanism of action.

References

1. Chenyu Zhu, Lei Gao, Yulun Wu, Yu-Hao Gu, Xinyu Xu, Ya Yin, Hai-Xu Wang, Shuai Yuan; Graphite-conjugated phthalocyanines through dioxin linkages: a molecularly programmable platform for heterogeneous CO2 electrocatalysis. Chem. Sci. (2026); https://doi.org/10.1039/d6sc06126e
2. Wu, H., Geng, Q., He, X., Zhang, M., & Maksimenko, S. (2026). Recent Advances in Metal Phthalocyanine for Sensing Applications. Nanomaterials, 16(5), 312. https://doi.org/10.3390/nano16050312
3. Lo, P. C., Rodríguez-Morgade, M. S., Pandey, R. K., Ng, D. K., Torres, T., & Dumoulin, F. (2020). The unique features and promises of phthalocyanines as advanced photosensitisers for photodynamic therapy of cancer. Chemical Society Reviews, 49(4), 1041-1056.
4. Baccani, I., Cuffari, S., Giuliani, F., Rossolini, G. M., & Pollini, S. (2025). Antimicrobial photodynamic activity of the zinc(II) phthalocyanine RLP068/Cl versus antimicrobial resistant priority pathogens. International Journal of Molecular Sciences, 26(15), 7545. https://doi.org/10.3390/ijms26157545

5. Gamelas, S. R. D., Bartolomeu, M., Vieira, C., Faustino, M. A. F., Tomé, J. P. C., Almeida, A., & Lourenço, L. M. O. (2024). Bacterial photodynamic inactivation mediated by pyridinium pyrazolyl zinc(II) phthalocyanines. ACS Applied Bio Materials, 7(11), 7748 – 7757. https://doi.org/10.1021/acsabm.4c01368
6. Karakılıç, E., et al. (2022). A versatile study of novel A_3B type unsymmetric zinc(II) phthalocyanines containing thiazolidin-4-one: Their carbonic anhydrase I, II isoenzymes and xanthine oxidase inhibitors evaluation. Journal of Molecular Structure, 1257, 132630. https://doi.org/10.1016/j.molstruc.2022.132630
7. Şahin, S., & Ağar, E. (2020). A_3B type unsymmetrical and amphiphilic phthalocyanines: Synthesis, characterization, thermal stability and aggregation studies. Spectrochimica Acta Part A: Molecular and Biomolecular Spectroscopy, 227, 117694. https://doi.org/10.1016/j.saa.2019.117694
8. Misir, M., Bilgin, A., Doyduk, D., & Demir, E. (2026). Novel polymer supported phthalocyanine nanosensors and analytical application. Topics in Catalysis, 69(1), 63-76.
9. Al-Bahrani, H.A., Kareem, M.M., Kadhum, A.A., Alrazzak, N.A.: Synthesis and characterization of new zinc phthalocyanine-dode¬cenyl succinic anhydride benzoic groups. Curr. Org. Synth. 17(6), 488 – 495 (2020)
10. El-Barasi, M. N., Algazale, F., S., El-Ajaily, M., Maihub, A., Miloud, M., Al-Noor, H.,T., Mubarak ,A., H. ., & Kareem, M., M. (2023). Synthesis, characterization, theoretical study and biological evaluation of Schiff base and their La(III), Ce(IV) and UO2(II) complexes. Bulletin of the Chemical Society of Ethiopia, 37(2), 335 – 346. https://doi.org/10.4314/bcse.v37i2.7
11. Salleh, M. Z., Nik Mohd Zuraina, N. N., Zainy Deris, Z., & Mohamed, Z. (2025). Current trends in the epidemiology of multidrug-resistant and beta-lactamase-producing Pseudomonas aeruginosa in Asia and Africa: A systematic review and meta-analysis. PeerJ, 13, e18986. https://doi.org/10.7717/peerj.18986
12. Spesia, M. B., & Durantini, E. N. (2022). Evolution of phthalocyanine structures as photodynamic agents for bacteria inactivation. Chemical Record, 22(4), e202100292. https://doi.org/10.1002/tcr.202100292
13. Safonova, E. A., Kolomeychuk, F. M., Gvozdev, D. A., Tsivadze, A. Y., & Gorbunova, Y. G. (2023). Tuning Photochemical and Photophysical Properties of P (V) Phthalocyanines. Molecules, 28(3), 1094.
14. Pasquina-Lemonche, L., Burns, J., Turner, R. D., Kumar, S., Tank, R., Mullin, N., Wilson, J. S., Chakrabarti, B., Bullough, P. A., Foster, S. J., & Hobbs, J. K. (2020). The architecture of the Gram-positive bacterial cell wall. Nature, 582(7811), 294 – 297. https://doi.org/10.1038/s41586-020-2236-6
15. Yıldız, B., Koca, A., & Erdoğmuş, A. (2022). Alkyl chain modified metallophthalocyanines with enhanced antioxidant and antimicrobial properties by doping Ag^{+} and Pd^{2+} ions. Journal of Molecular Structure, 1257, 132634. https://doi.org/10.1016/j.molstruc.2022.132634
16. Kalkan, A., Yıldız, B., & Erdoğmuş, A. (2023). Photoantimicrobial activity of Schiff-base morpholino phthalocyanines against drug-resistant microorganisms. Photodiagnosis and Photodynamic Therapy, 42, 103519. https://doi.org/10.1016/j.pdpdt.2023.103519
17. Magadla, A., Openda, Y. I., Mpeta, L. S., & Nyokong, T. (2023). Evaluation of the antibacterial activity of gallic acid anchored phthalocyanine-doped silica nanoparticles towards Escherichia coli and Staphylococcus aureus biofilms and planktonic cells. Photodiagnosis and Photodynamic Therapy, 42, 103520
18. Zhao, P., Song, Y., Dong, S., Niu, L., & Zhang, F. (2009). Synthesis, photophysical and photochemical properties of amphiphilic carboxyl phthalocyanine oligomers. Dalton Transactions, (32), 6327-6334.
19. Uğur, A. L., Dinçer, H. A., & Erdoğmuş, A. (2012). Synthesis, photophysical and thermal studies of symmetrical and unsymmetrical zinc phthalocyanines. Polyhedron, 31(1), 431-437.
20. Sen, P., Yildiz, S. Z., Erdoğmuş, A., Dege, N., & Atalay, Y. (2016). Aldehyde substituted phthalocyanines: Synthesis, characterization and investigation of photophysical and photochemical properties. Journal of Fluorescence, 26(4), 1521 – 1534.
21. Saldívar‐Guerra, E., & Vivaldo‐Lima, E. (2025). Introduction to polymers and polymer types. Polymer Science, Engineering, and Sustainability, 1, 1-18.
22. Pasieczna-Patkowska, S., Cichy, M., & Flieger, J. (2025). Application of Fourier transform infrared (FTIR) spectroscopy in characterization of green synthesized nanoparticles. Molecules, 30(3), 684. https://doi.org/10.3390/molecules30030684
23. Pretsch, E., Bühlmann, P., & Badertscher, M. (2020). Structure determination of organic compounds: Tables of spectral data (4th ed.). Springer. https://doi.org/10.1007/978-3-662-62470-9
24. Chambrier, I., Cook, M. J., Mayes, D. A., & MacDonald, C. (2003). NMR spectroscopic evidence for the self-association of some asymmetrically substituted phthalocyanines in solution. Journal of Porphyrins and Phthalocyanines, 7(6), 426 – 438.
25. Souza, T. F. D., Antonio, F. C., Zanotto, M., Homem-de-Mello, P., & Ribeiro, A. O. (2018). Photophysical and photochemical properties and aggregation behavior of phthalocyanine and naphthalocyanine derivatives. Journal of the Brazilian Chemical Society.
26. Apostol, P., Bentaleb, A., Rajaoarivelo, M., Clérac, R., & Bock, H. (2015). Regiospecific synthesis of tetrasubstituted phthalocyanines and their liquid crystalline order. Dalton Transactions, 44, 5569 – 5576. https://doi.org/10.1039/C5DT00076A

27. Gregson, A. K., Martin, R. L., & Mitra, S. (1976). Paramagnetic anisotropy of planar cobalt(II) and copper(II) phthalocyanine, bis(pentane-2,4-dionato)copper(II), and bis(pentane-2,4-dithionato)cobalt(II). Journal of the Chemical Society, Dalton Transactions, 1458 – 1466. https://doi.org/10.1039/DT9760001458
28. Tkachenko, N., Golovanov, V., Penni, A., Vesamäki, S., Ajayakumar, M. R., Muranaka, A., Kobayashi, N., & Efimov, A. (2024). The windmill, the dragon, and the frog: geometry control over the spectral, magnetic, and electrochemical properties of cobalt phthalocyanine regioisomers. Physical Chemistry Chemical Physics, 26, 18113 – 18128. https://doi.org/10.1039/D4CP01564A
29. Burat, A. (2020). α -and β -substituted metal-free phthalocyanines: synthesis, photophysical and electrochemical properties. Molecules, 25(2), 363.
30. Matson, J. B., Steele, A. Q., Mase, J. D., & Schulz, M. D. (2024). Polymer characterization by size-exclusion chromatography with multi-angle light scattering (SEC-MALS): a tutorial review. Polymer chemistry, 15(3), 127-142.
31. Murad, D. M. A., Al-Mayyahi, B. A., & Abbas, A. F. (2025). Synthesis and characterization of new fluorescence polyamides. New Materials, Compounds and Applications, 9(2), 1 – 17. https://doi.org/10.62476/nmca.92309

Preparation of the maleimide-functionalized phthalonitrile precursor

Maleic anhydride (3.268 g) and 4-aminophthalonitrile (4.771 g) were mixed in DMF (10 mL), and phosphoric acid (H_3PO_4; 2–3 drops) was added. The mixture was heated under reflux with stirring for 2 h. The reaction mixture was then added to cold distilled water, and the resulting product was recrystallized from ethanol to obtain 4-(2,5-dioxo-2,5-dihydro-1H-pyrrol-1-yl)phthalonitrile.

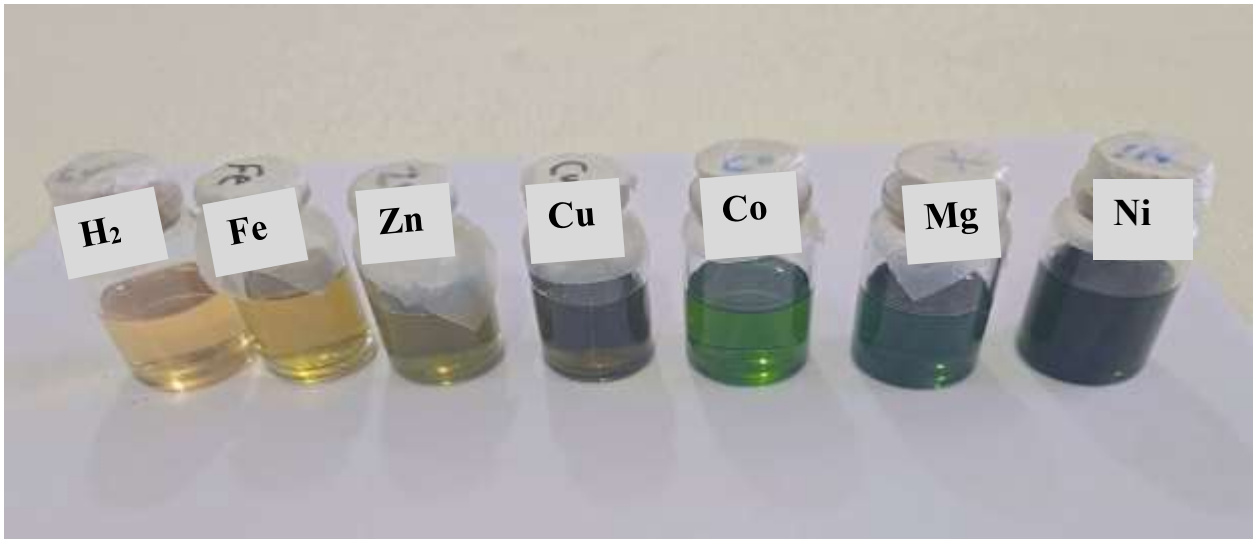


Figure S1. Colours of monomeric phthalocyanines 1–7.

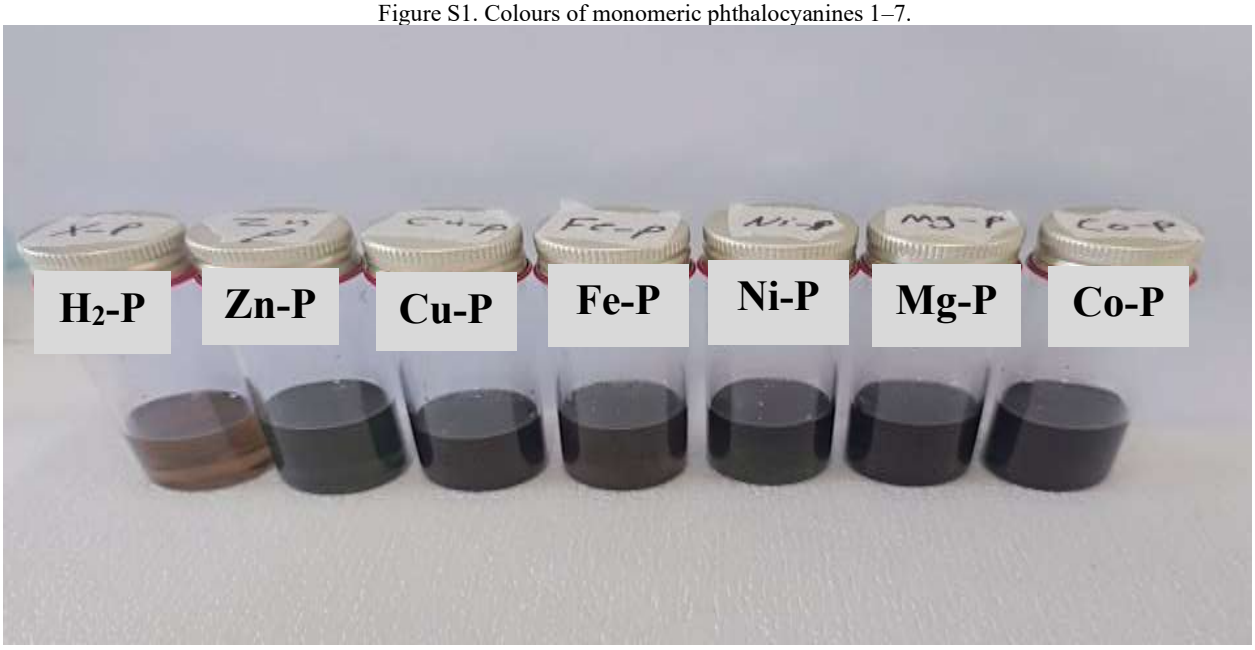


Figure S2. Colours of polymeric phthalocyanines 8–14.

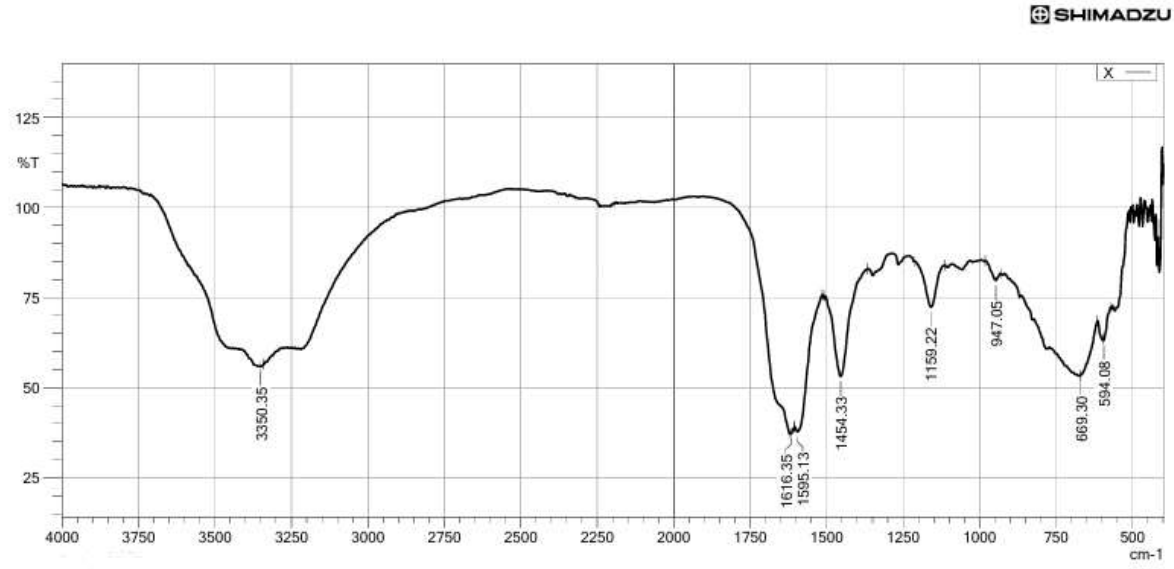


Figure S3. FT-IR spectrum of compound 1 (Pc–H_2).

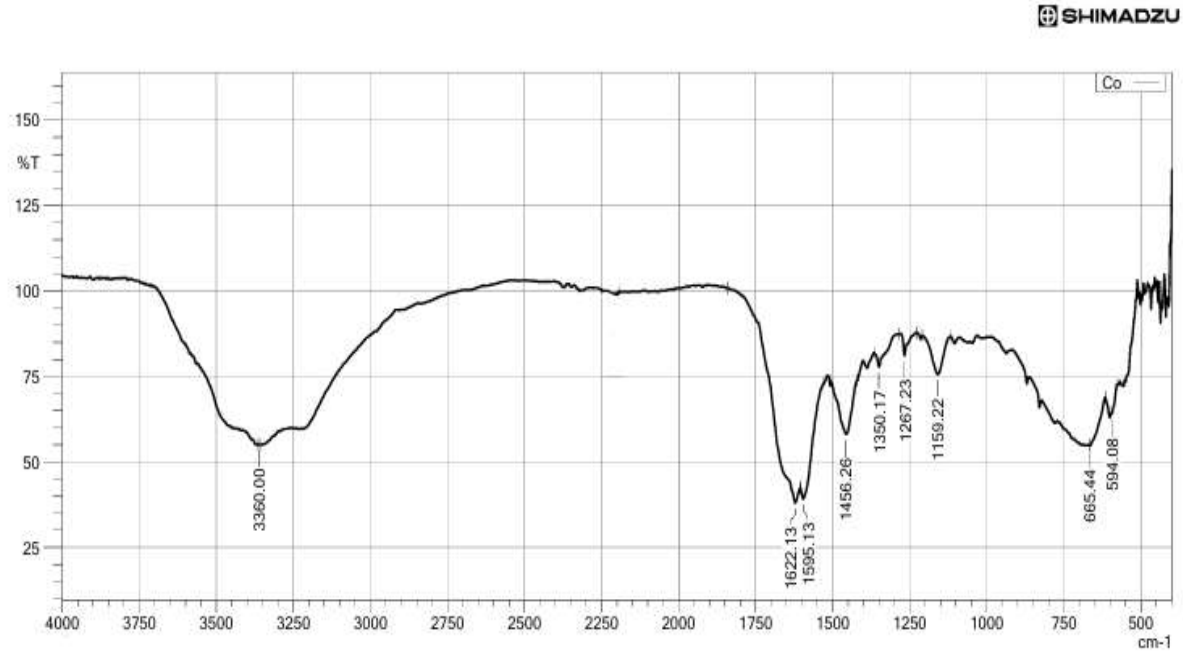


Figure S4: FTIR spectrum for 2 (Pc- Co)

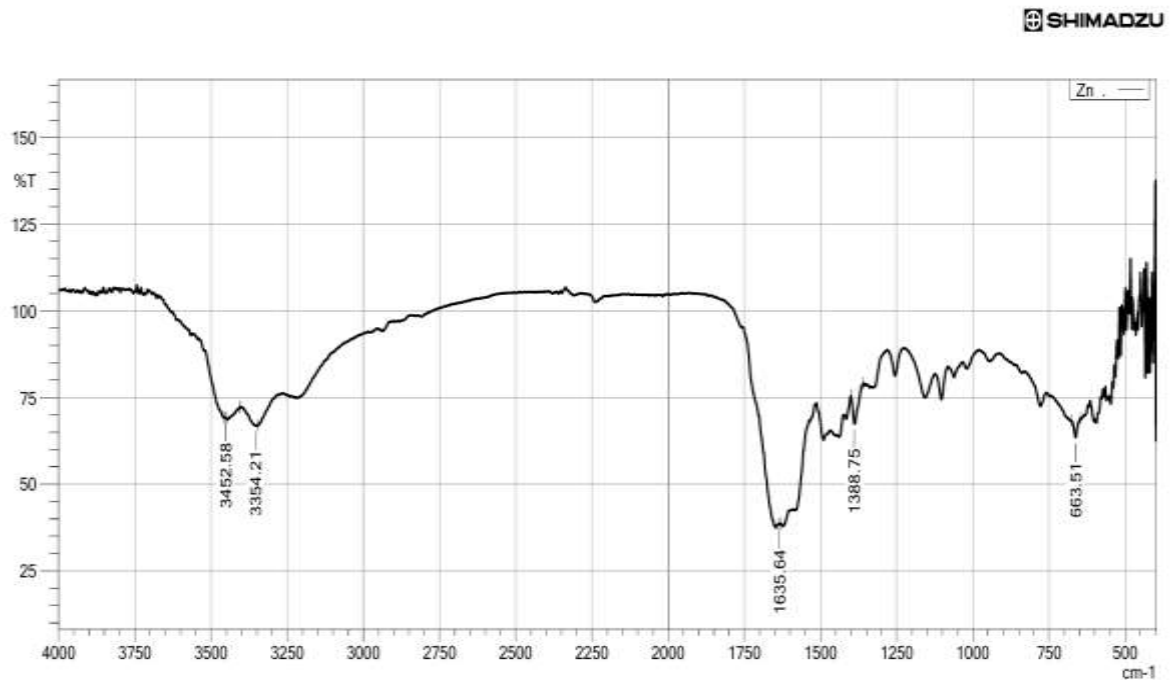


Figure S5. FT-IR spectrum of compound 3 (Pc–Zn).

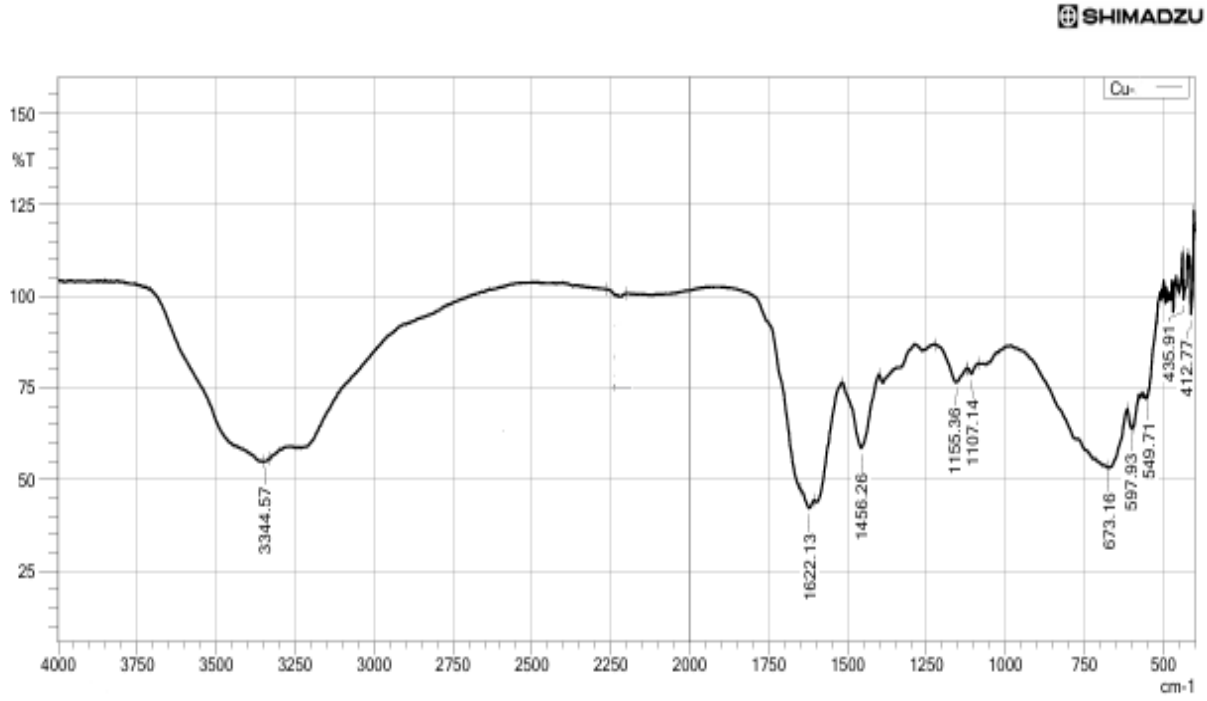


Figure S6. FT-IR spectrum of compound 4 (Pc–Cu).

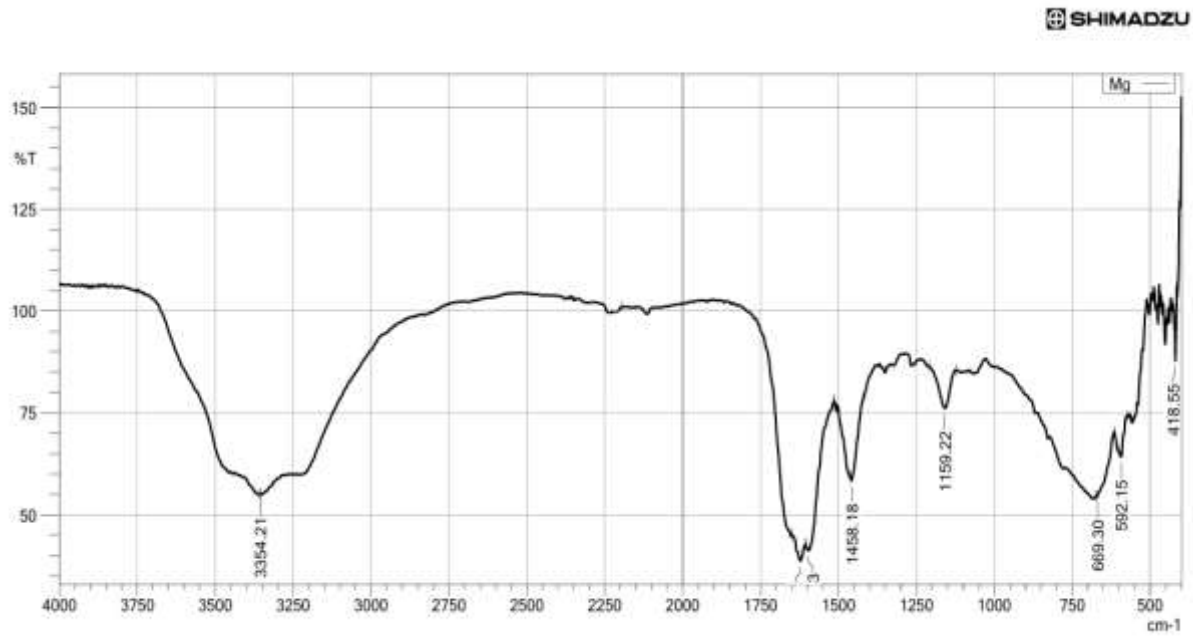


Figure S7. FT-IR spectrum of compound 5 (Pc–Mg).

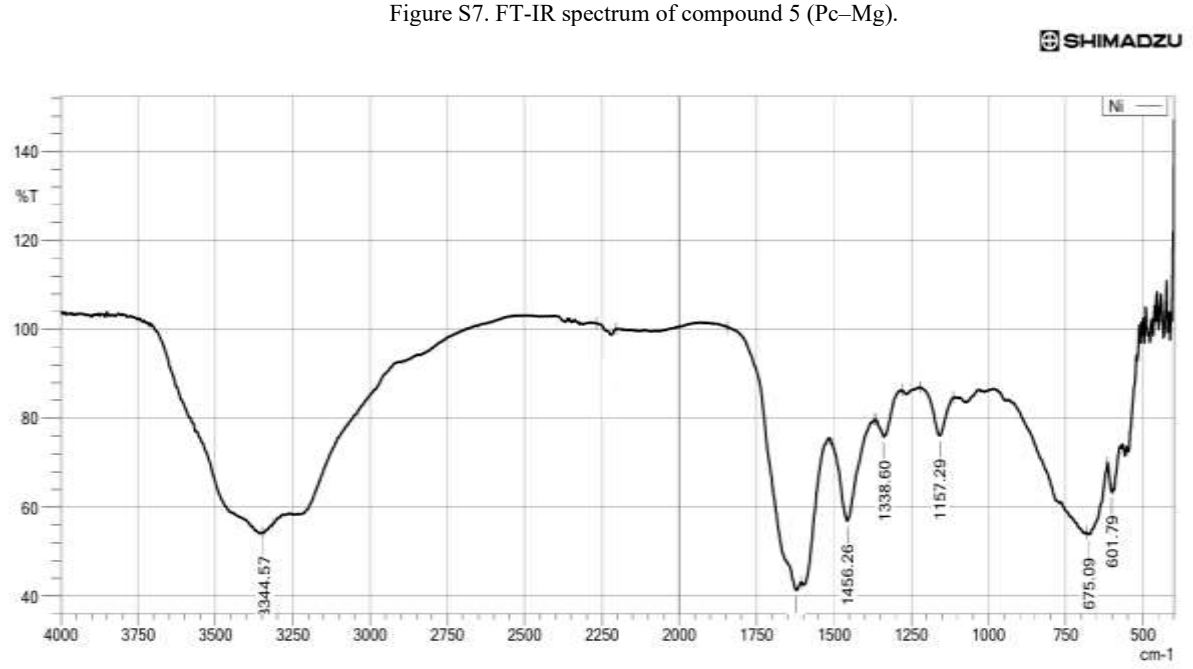


Figure S8. FT-IR spectrum of compound 6 (Pc–Ni).

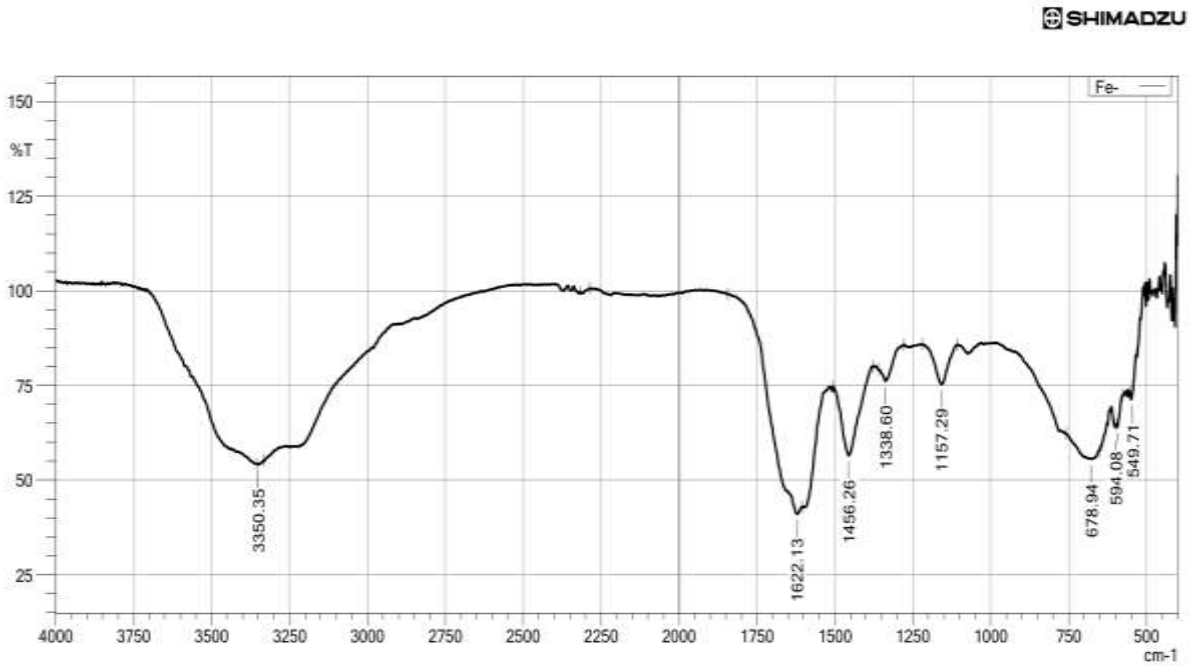


Figure S9. FT-IR spectrum of compound 7 (Pc–Fe).

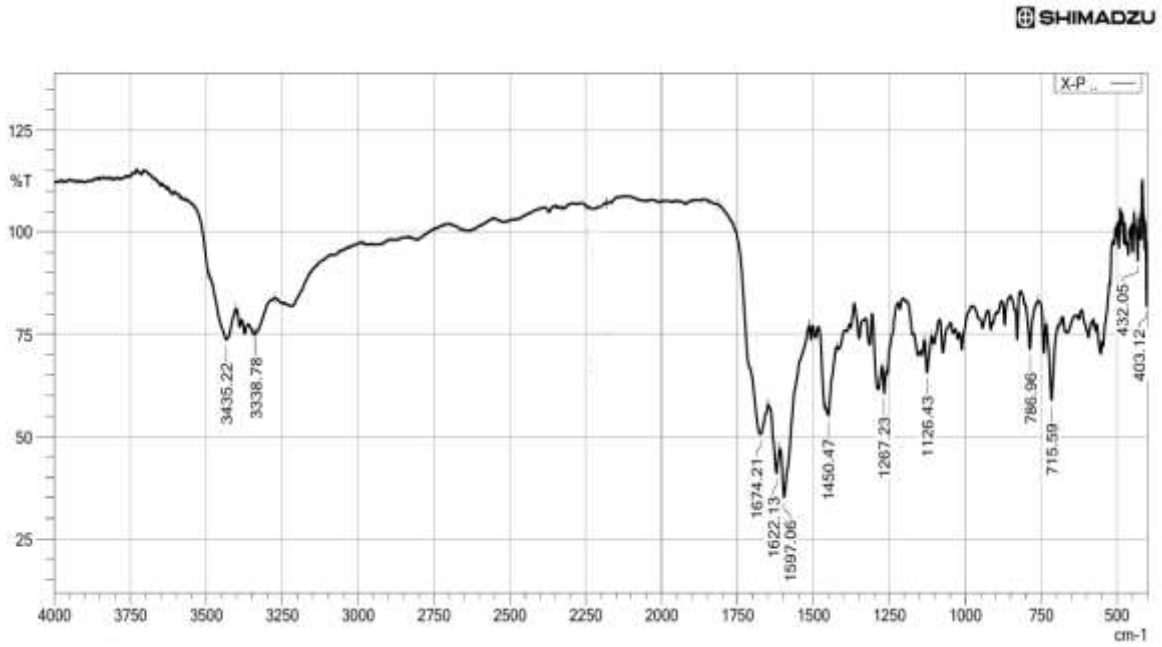


Figure S10. FT-IR spectrum of compound 8 (Polymer–H_2).

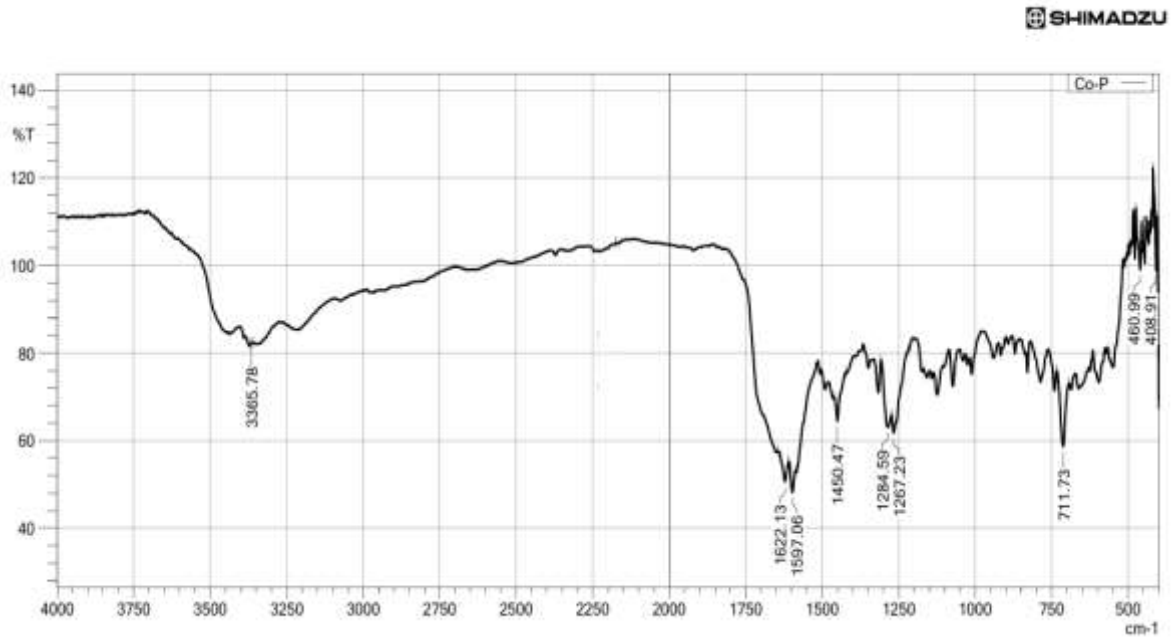


Figure S11. FT-IR spectrum of compound 9 (Polymer–Co).

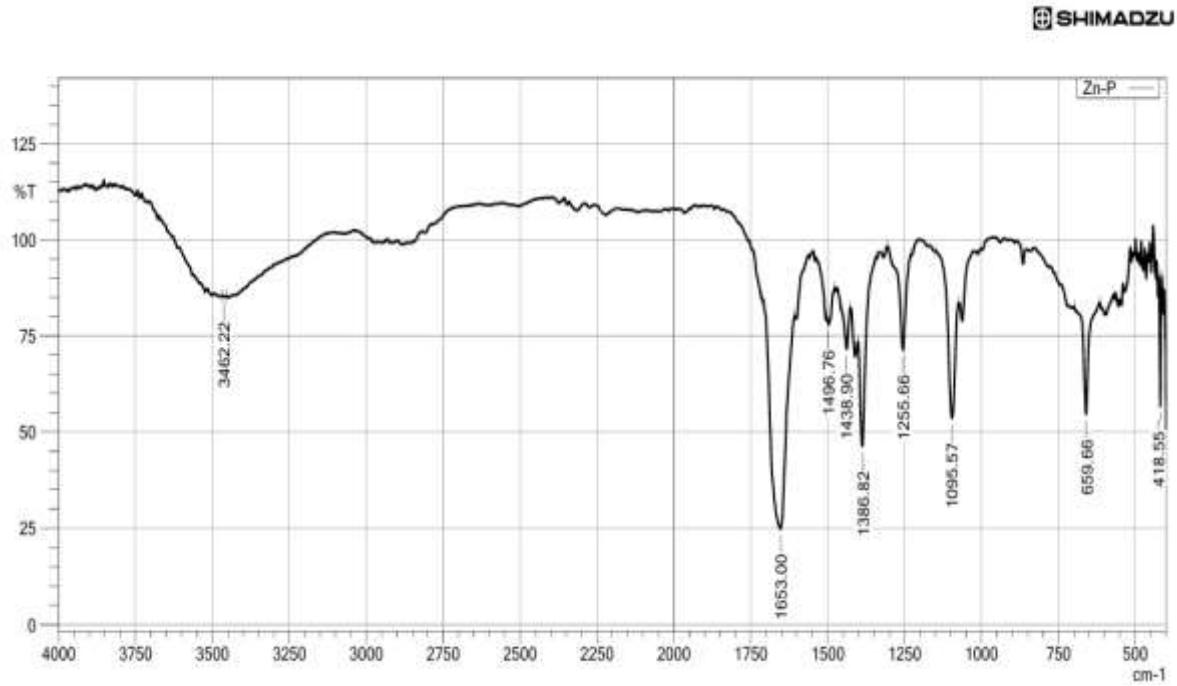


Figure S12. FT-IR spectrum of compound 10 (Polymer–Zn).

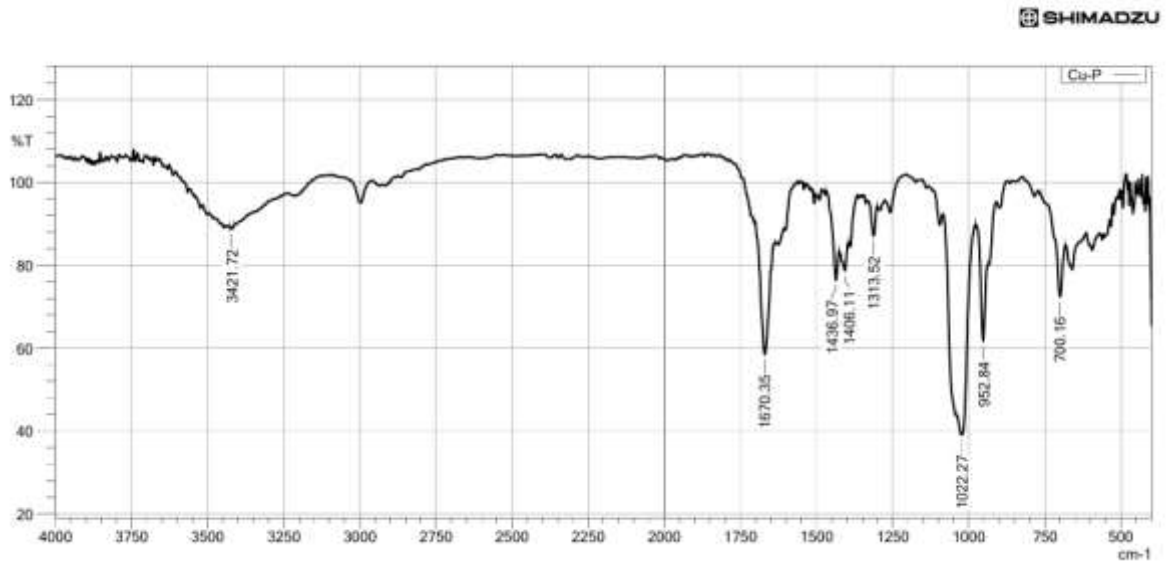


Figure S13. FT-IR spectrum of compound 11 (Polymer–Cu).

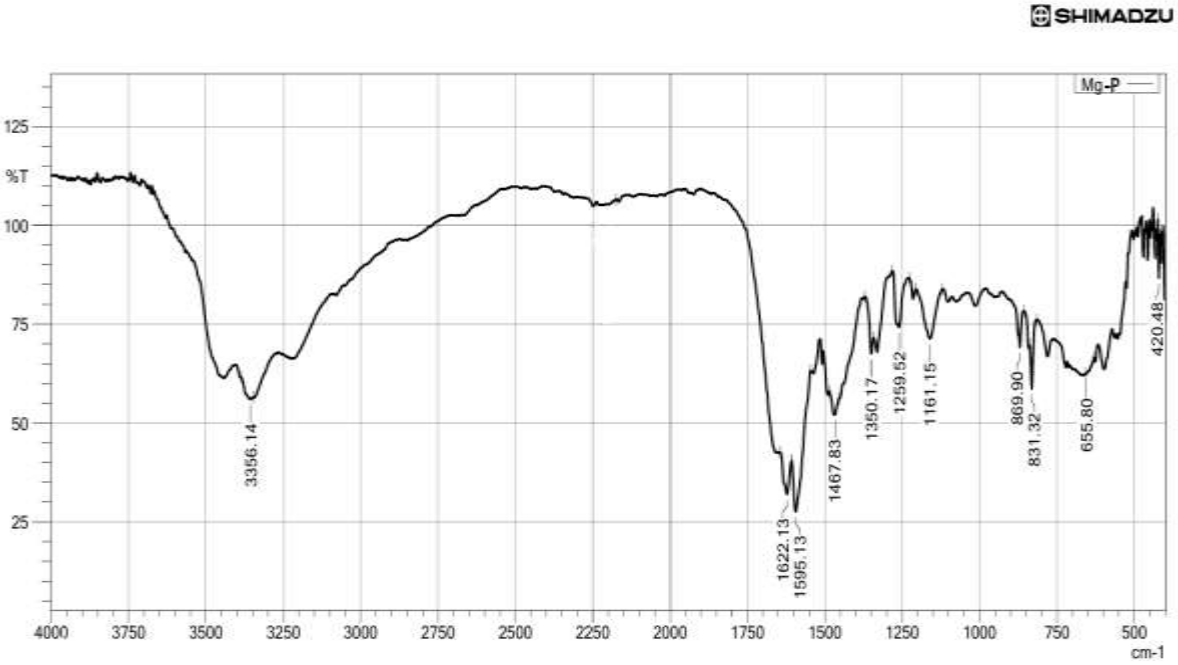


Figure S14. FT-IR spectrum of compound 12 (Polymer–Mg).

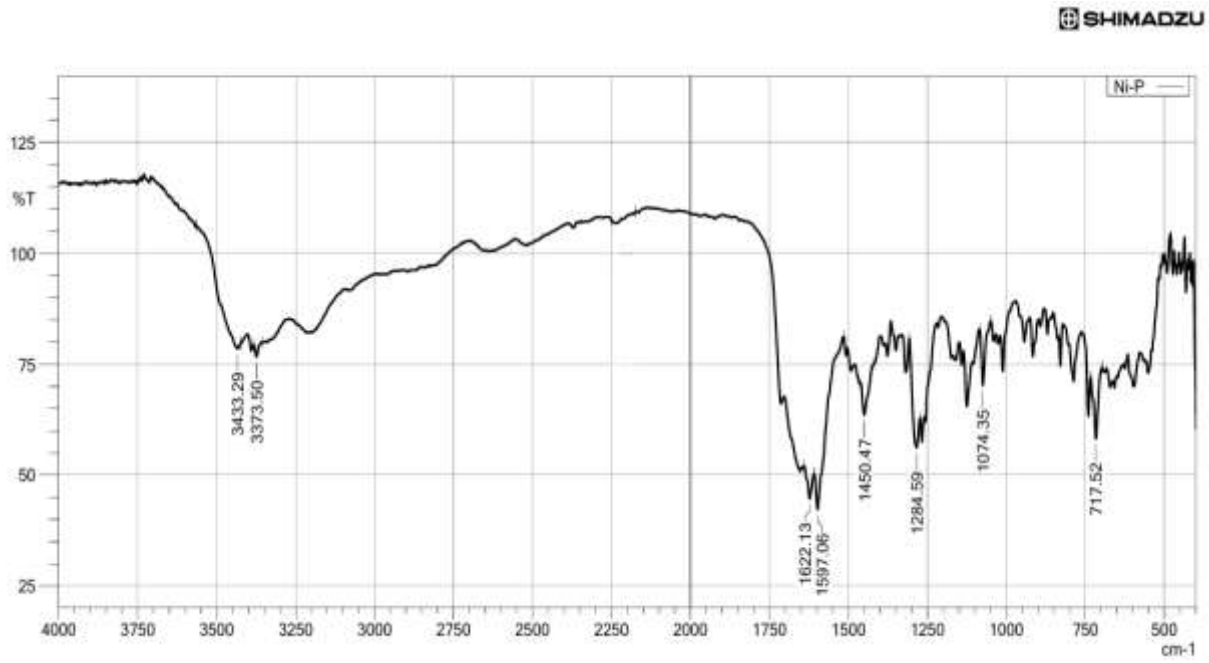


Figure S15. FT-IR spectrum of compound 13 (Polymer–Ni).

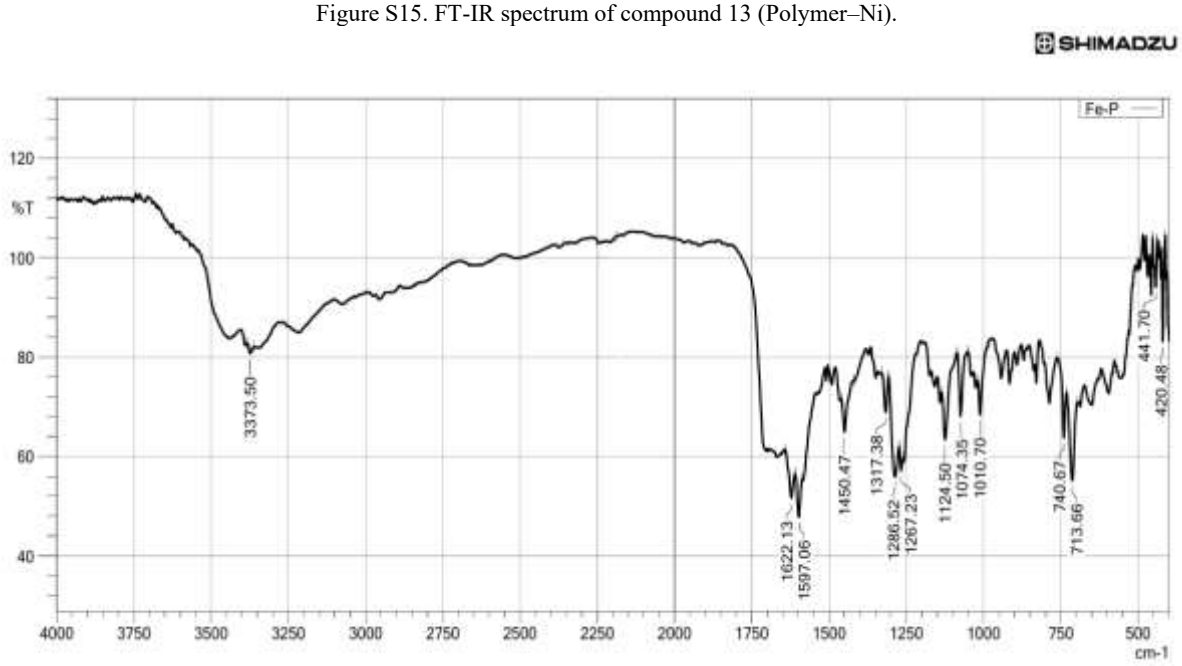


Figure S16. FT-IR spectrum of compound 14 (Polymer–Fe).

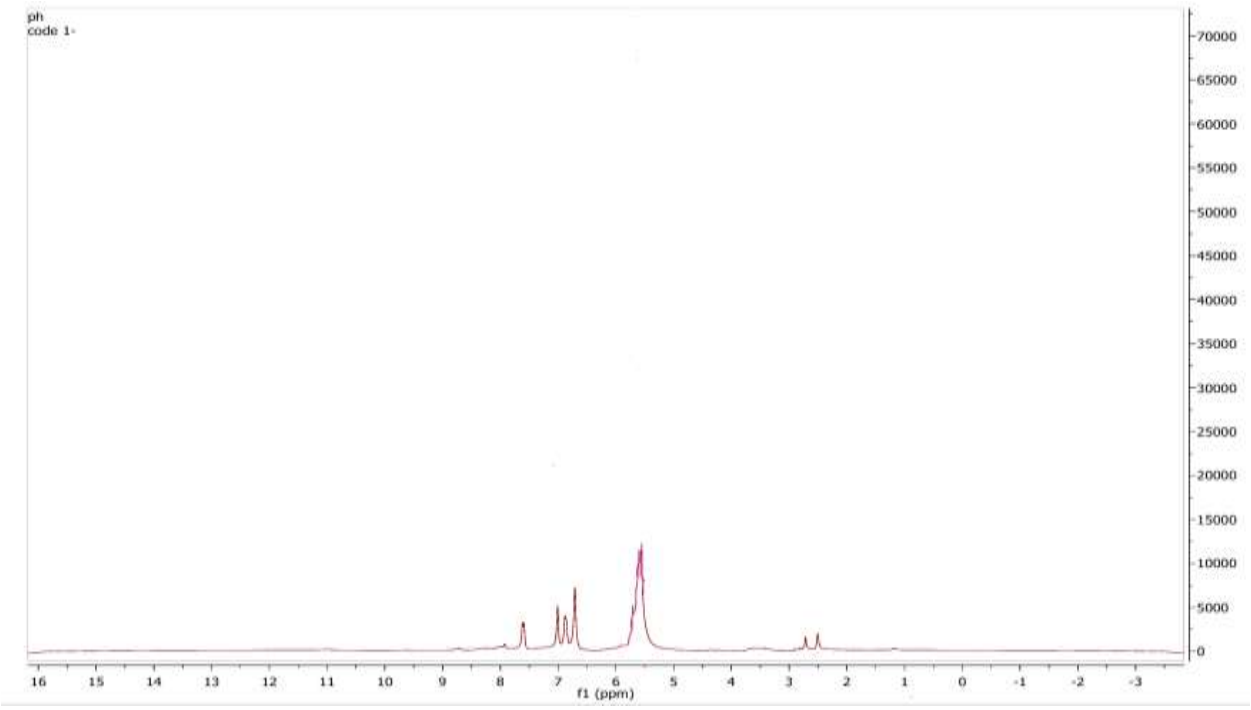


Figure S17. ^{1}H NMR spectrum of compound 1 (Pc–H_2).

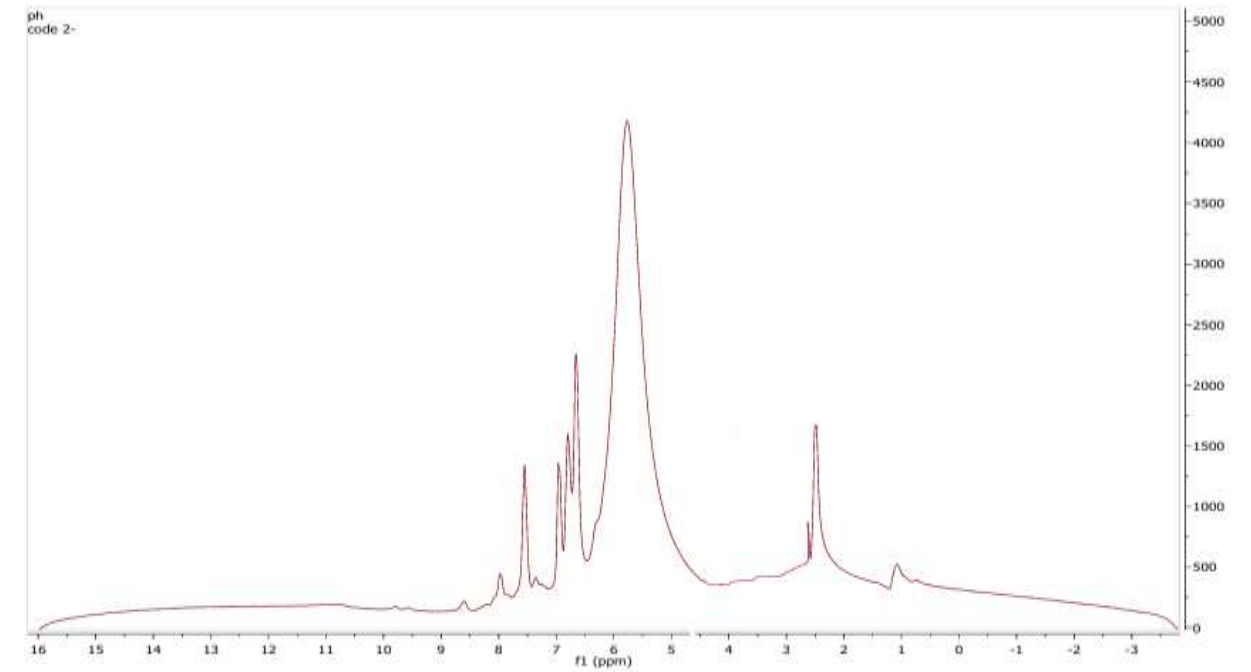


Figure S18. ^{1}H NMR spectrum of compound 2 (Pc–Co).

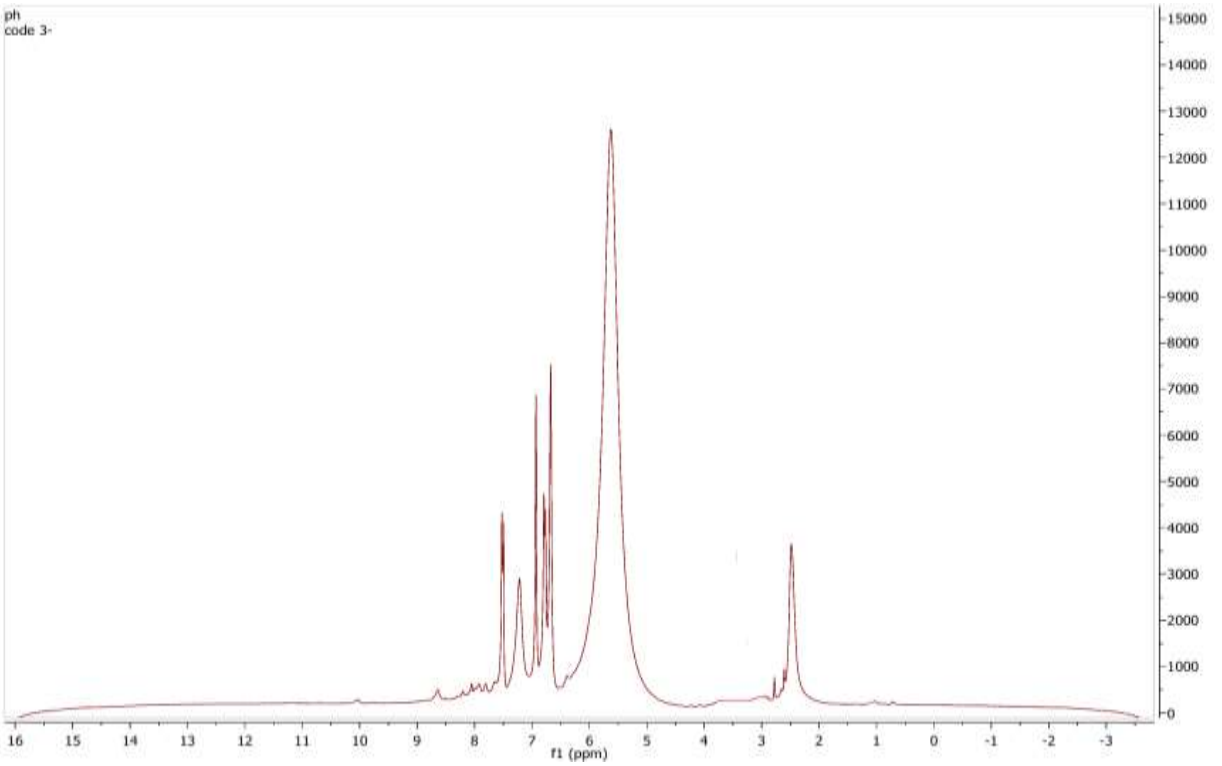


Figure S19. ^{1}H NMR spectrum of compound 3 (Pc–Zn).

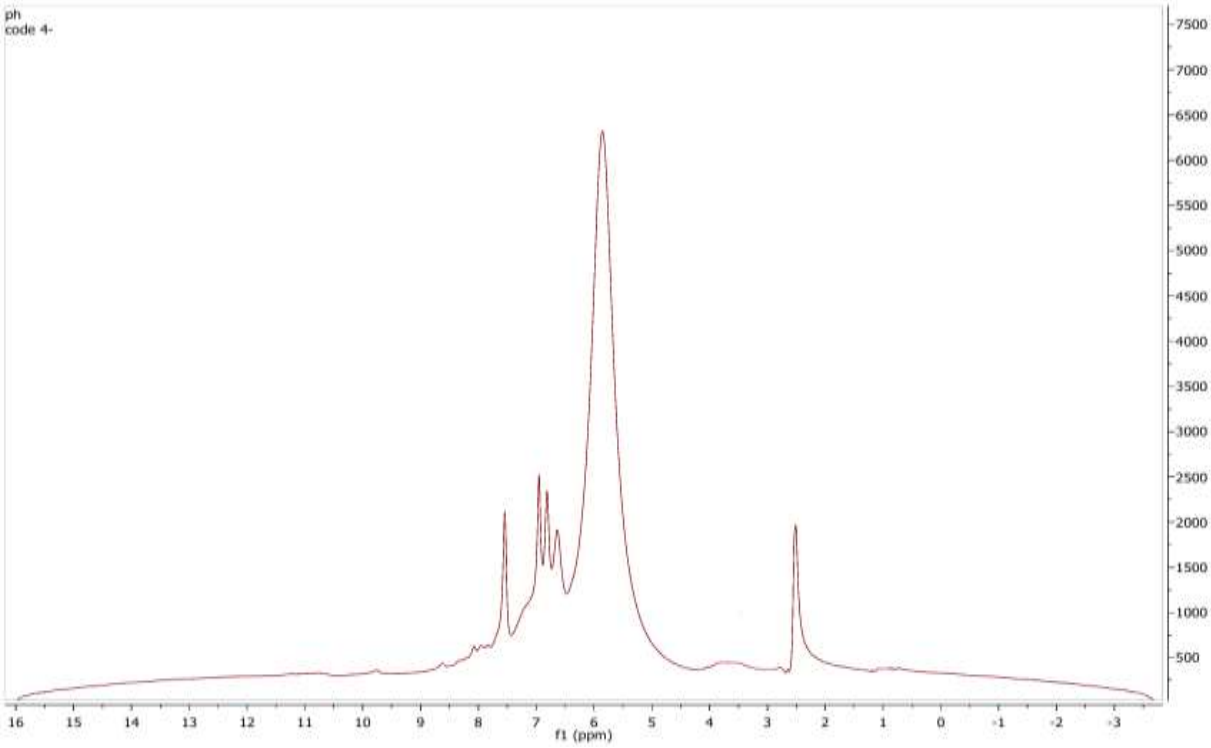


Figure S20. ^{1}H NMR spectrum of compound 4 (Pc–Cu).

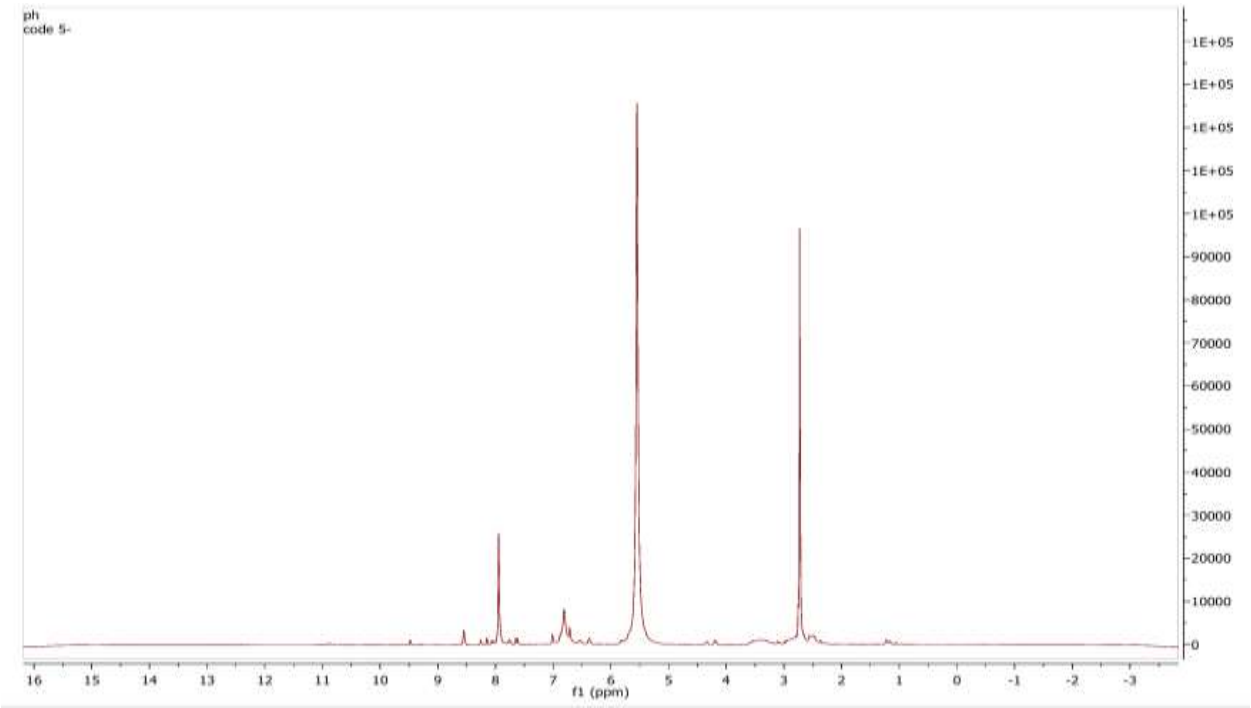


Figure S21. ^{1}H NMR spectrum of compound 5 (Pc–Mg).

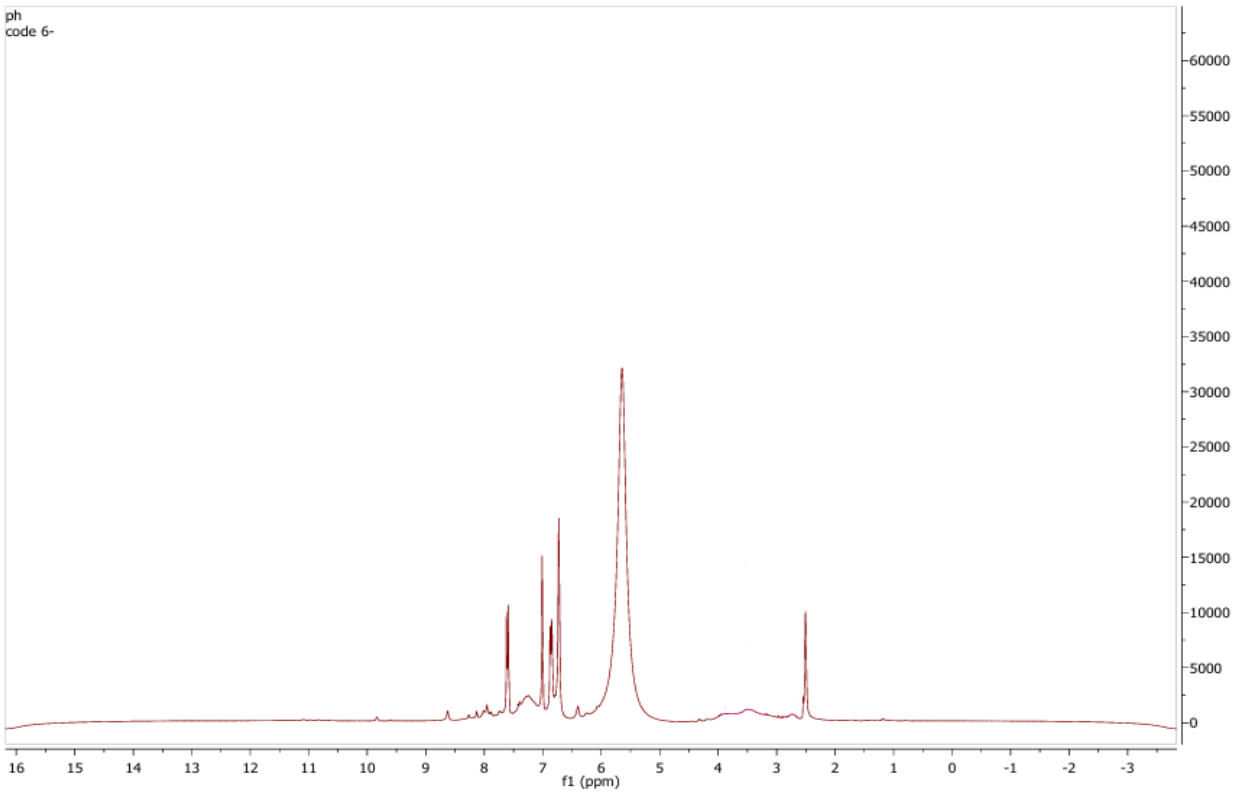


Figure S22. ^{1}H NMR spectrum of compound 6 (Pc–Ni).

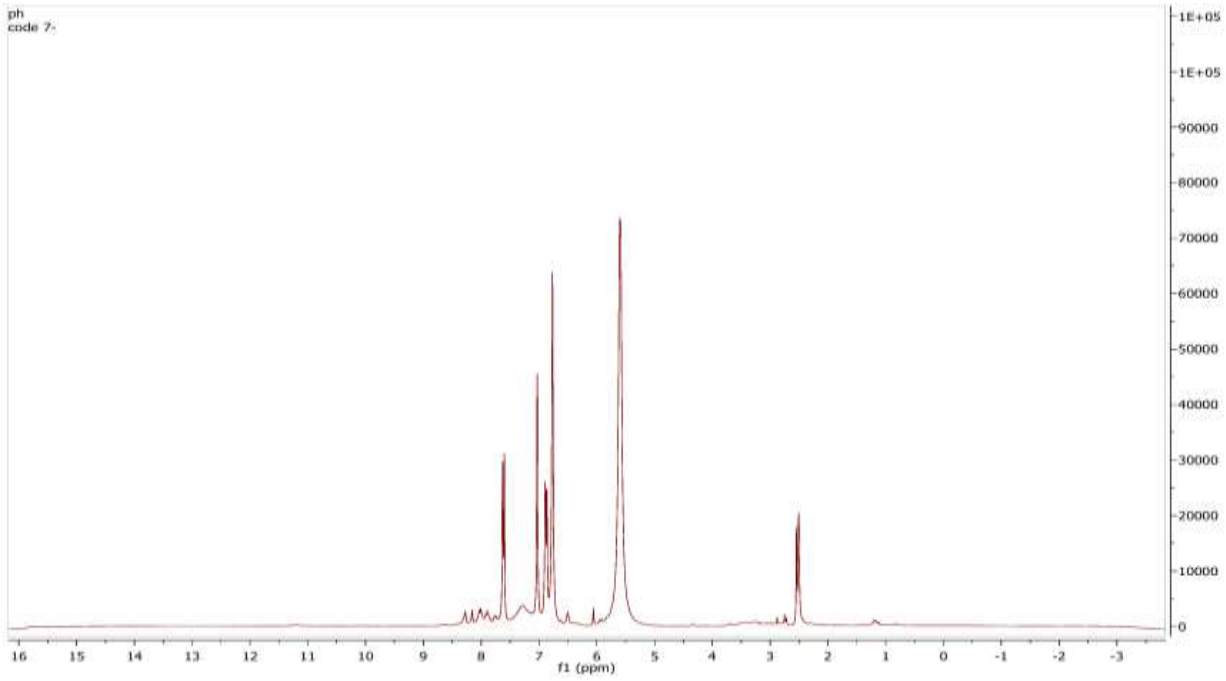
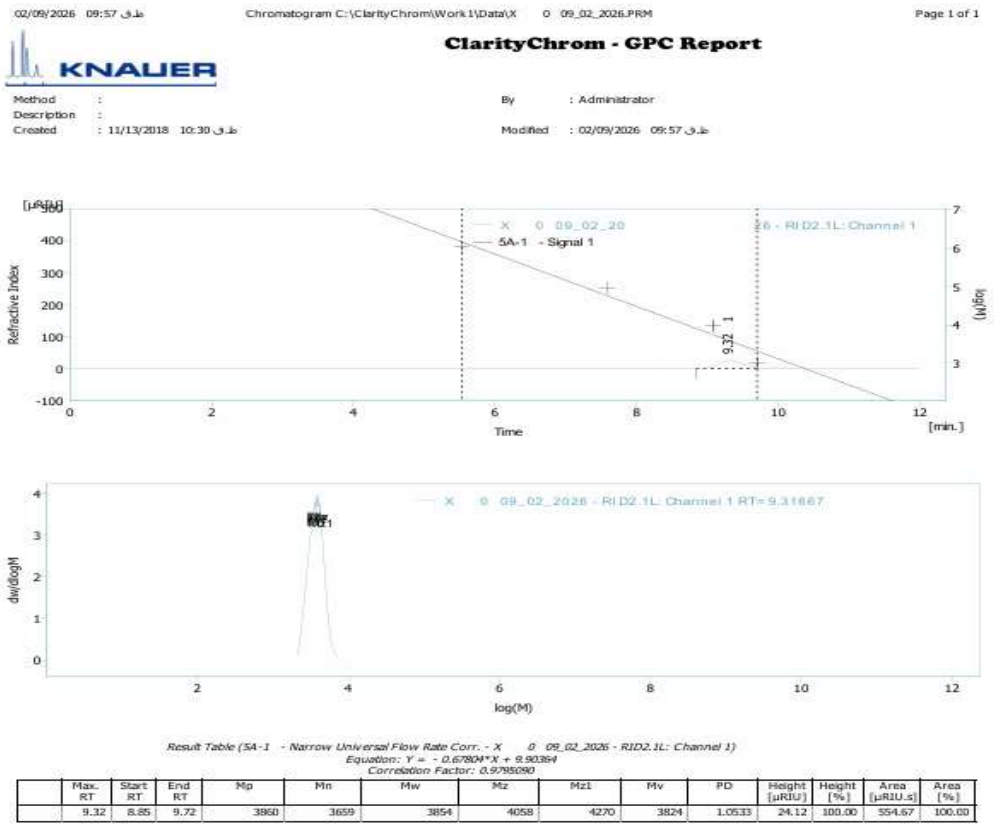


Figure S23. ^{1}H NMR spectrum of compound 7 (Pc–Fe).



	Max. RT	Start RT	End RT	Mp	Mn	Mw	Mz	Mz1	Mv	PD	Height [µRIU]	Height [%]	Area [µRIU.s]	Area [%]
	9.32	8.85	9.72	3860	3659	3854	4058	4270	3824	1.0533	24.12	100.00	554.67	100.00

Figure S24. GPC chromatogram of Polymer–H$_2$ (compound 8).

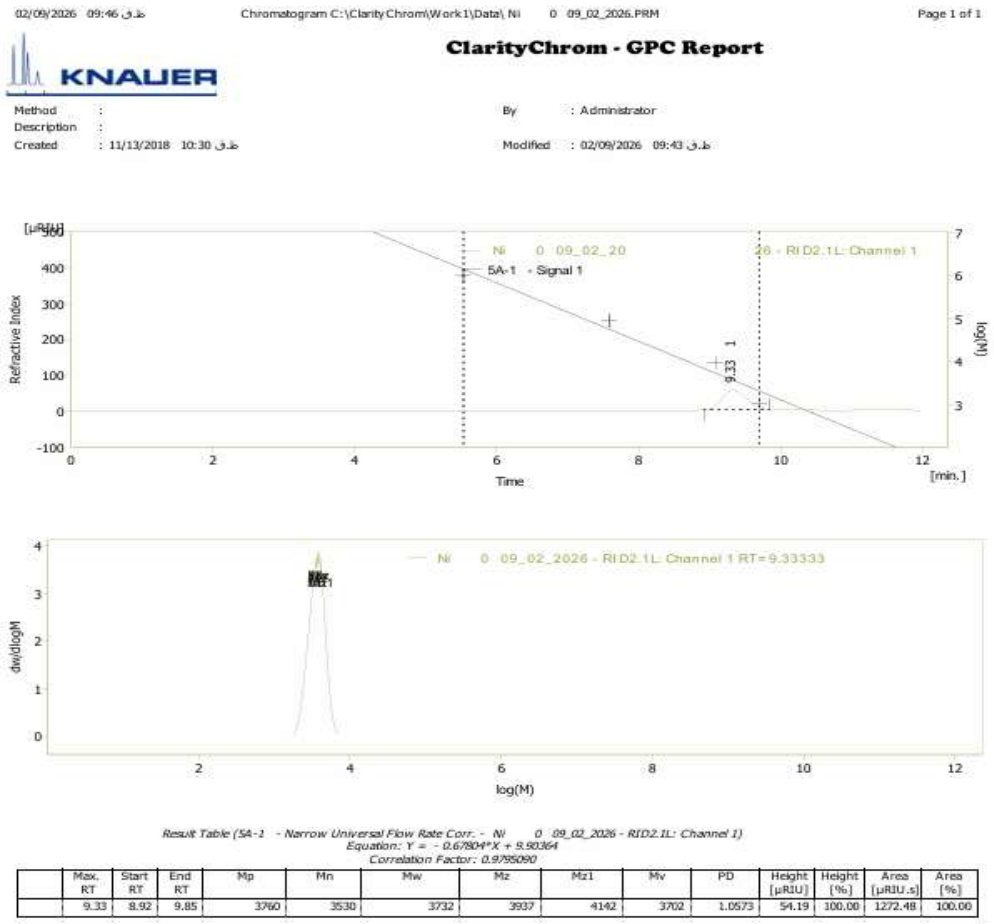


Figure S25. GPC chromatogram of Polymer–Ni (compound 13).

Table S1. Reported antibacterial inhibition-zone diameters for polymeric compounds 8–14.

Polymeric compound or reference antibiotic	*Staphylococcus aureus* (mm)	*Escherichia coli* (mm)
Ampicillin	21–28	14–16
Amoxicillin	22–24	14–19
Polymer–H_2 (8)	17	15
Polymer–Co (9)	15	15
Polymer–Zn (10)	10	10
Polymer–Cu (11)	15	18
Polymer–Mg (12)	10	12
Polymer–Ni (13)	12	13
Polymer–Fe (14)	15	15

Negative control: DMSO alone showed no detectable antibacterial activity against either *Staphylococcus aureus* or *Escherichia coli*.

Table S2: Electronic spectra of compounds 1-7

Compounds	Absorption Band ,nmλ	Transfers
(H_2)	694.5	π-π*
(Co)	676.0	π-π*
(Zn)	691.5	π-π*
(Cu)	679.0	π-π*
(Mg)	677.0	π-π*
(Ni)	695.0	π-π*
(Fe)	694.0	π-π*

Table S3: Electronic spectra of compounds 8-14

Compounds	Absorption Band ,nmλ	Transfers
Polymer (H_2)	697.0	π-π*
Polymer (Co)	696.5	π-π*
Polymer (Zn)	697.5	π-π*
Polymer (Cu)	700.0	π-π*
Polymer (Mg)	698.0	π-π*
Polymer (Ni)	695.5	π-π*
Polymer (Fe)	695.0	π-π*



Image S1. Antibacterial activity of polymeric compounds 8–14 against *Staphylococcus aureus*. Compound numbers 8–14 correspond to plate labels 4, 5, 8, 3, 6, 7, and 9, respectively.



Image S2. Antibacterial activity of polymeric compounds 8–14 against *Escherichia coli*. Compound numbers 8–14 correspond to plate labels 4, 5, 8, 3, 6, 7, and 9, respectively.

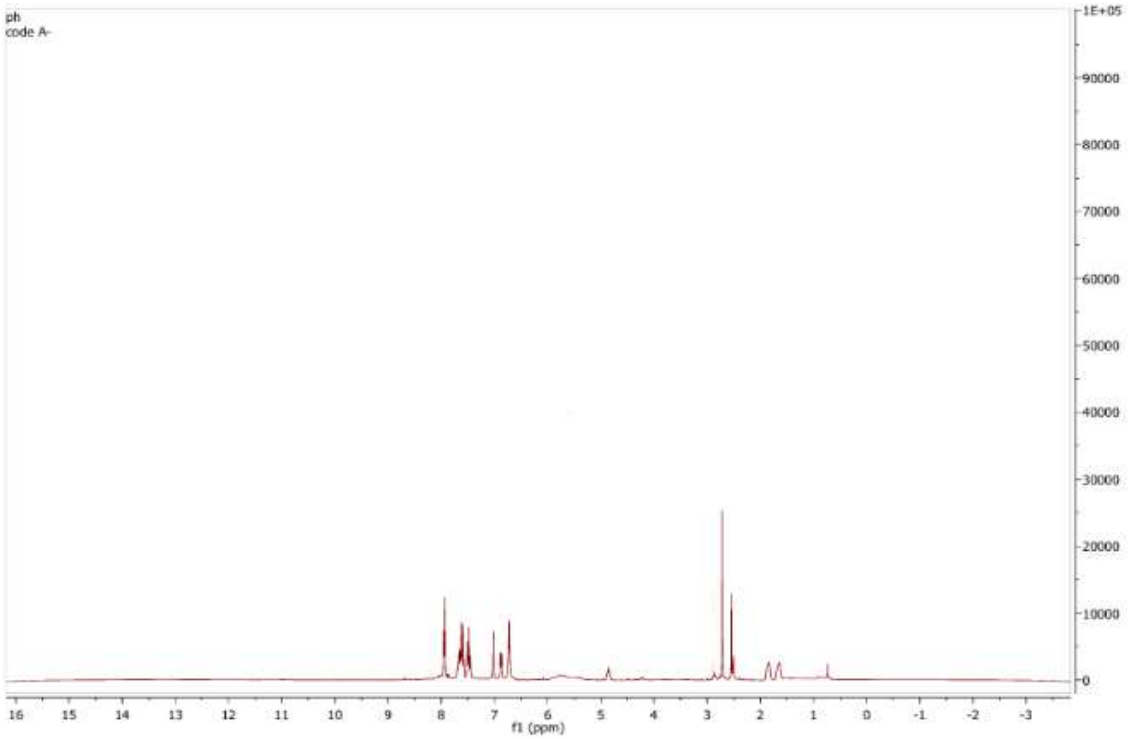


Figure S26. Supplied ^{1}H NMR spectrum of compound 8 (Polymer–H_2).

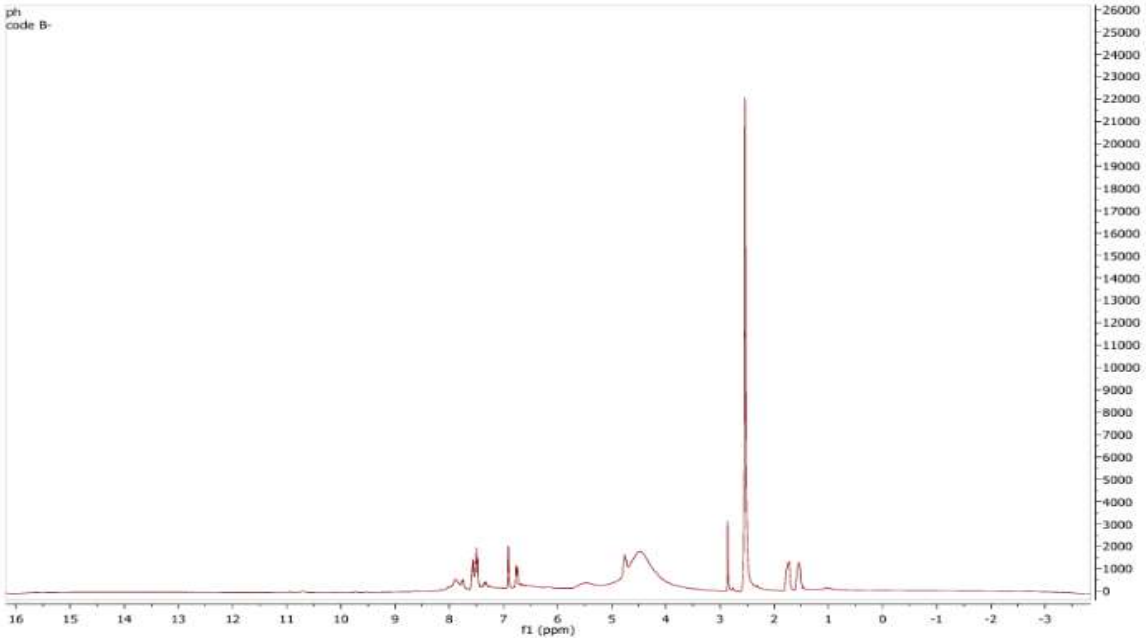


Figure S27. Supplied ^{1}H NMR spectrum of compound 9 (Polymer–Co).

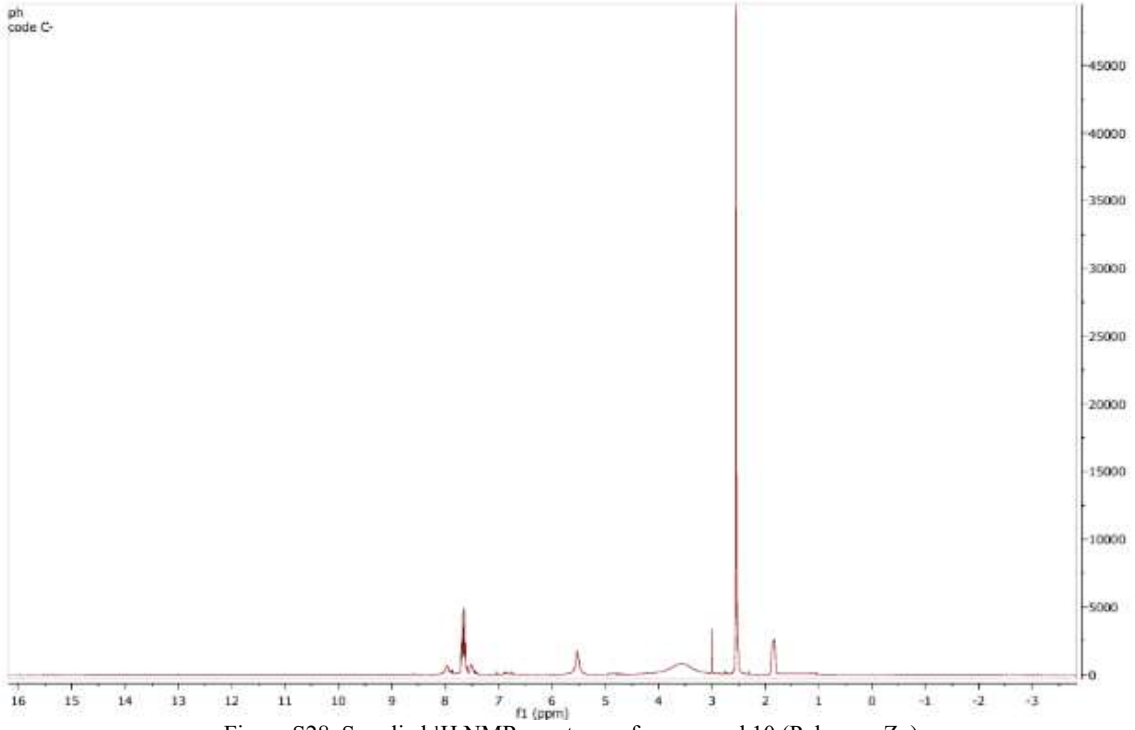


Figure S28. Supplied ^{1}H NMR spectrum of compound 10 (Polymer–Zn).

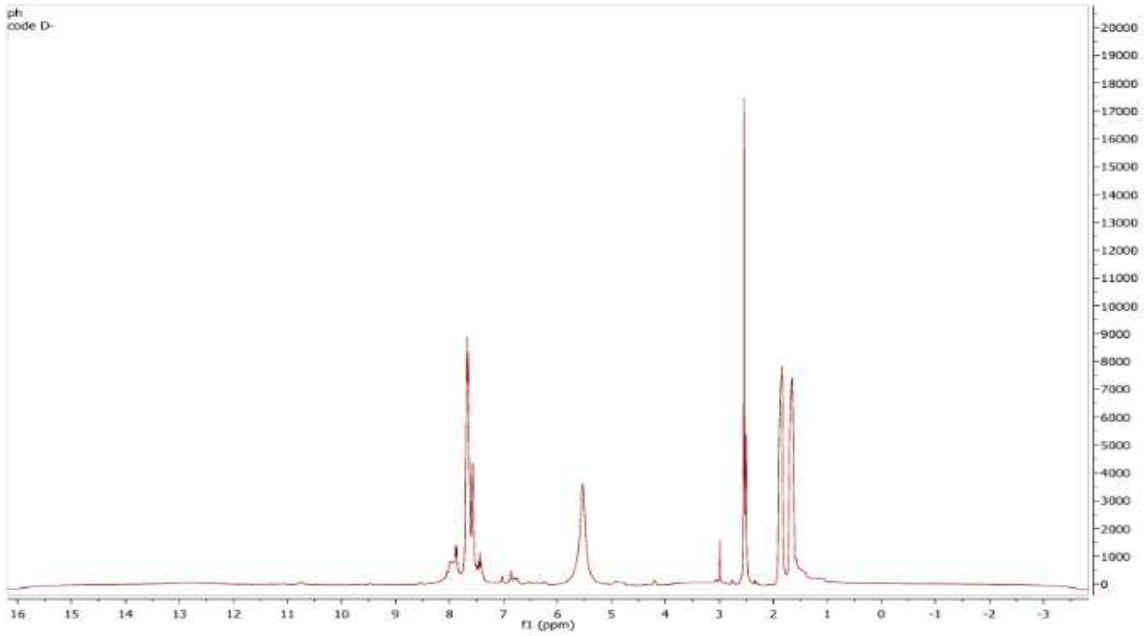


Figure S29. Supplied ^{1}H NMR spectrum of compound 11 (Polymer–Cu).

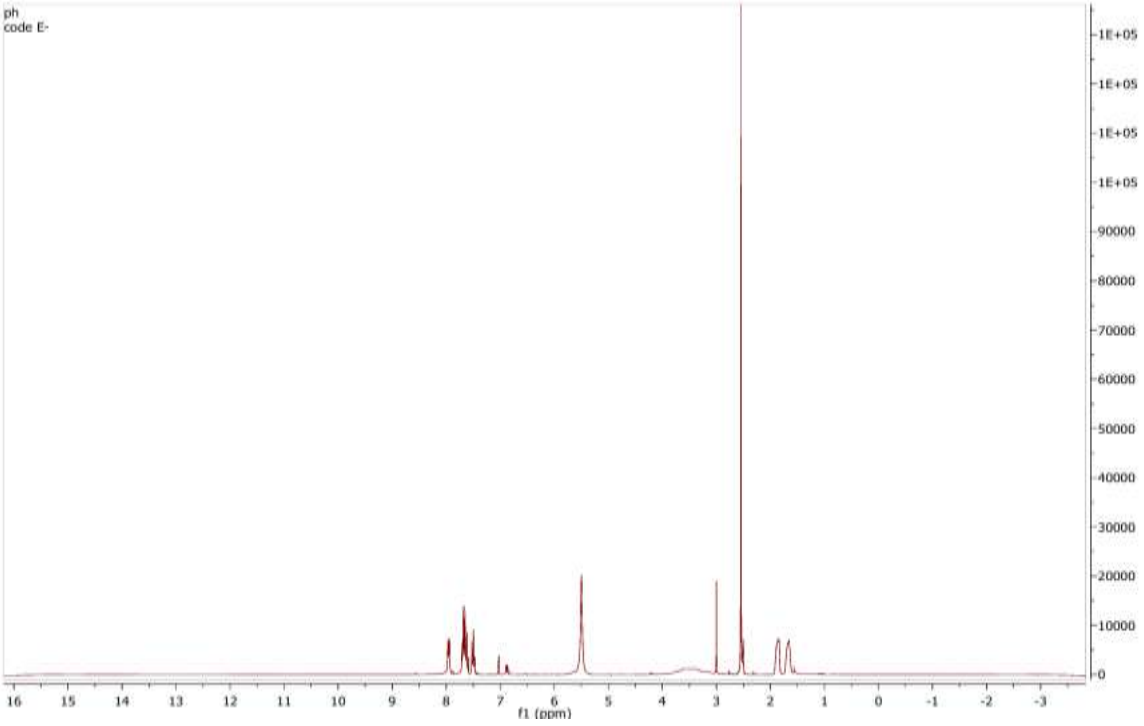


Figure S30. Supplied ^{1}H NMR spectrum of compound 12 (Polymer–Mg).

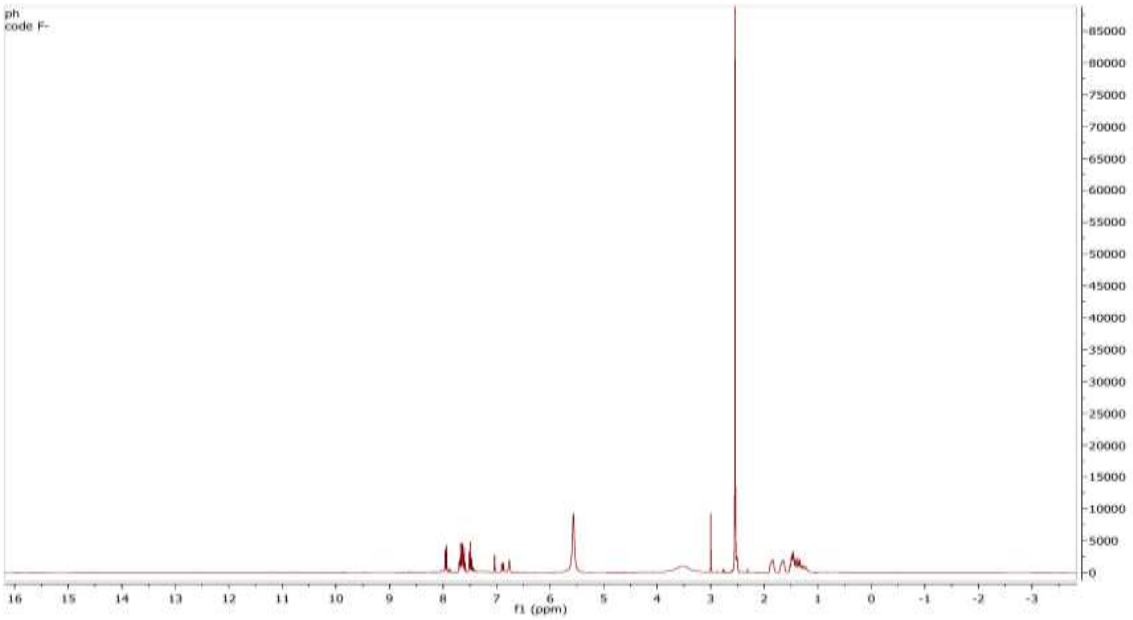


Figure S31. Supplied ^{1}H NMR spectrum of compound 13 (Polymer–Ni).

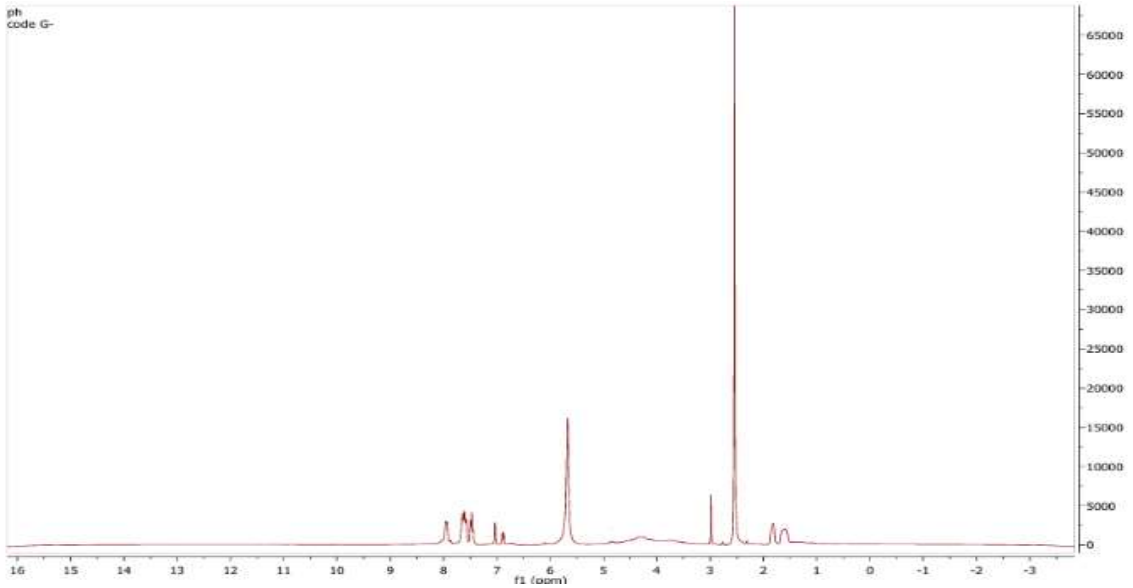


Figure S32. Supplied ^{1}H NMR spectrum of compound 14 (Polymer–Fe).